Fluorinated Peptide Hydrogels Result in Longer In Vivo Residence Time after Subcutaneous Administration

Aurélie Honfroy, Jolien Bertouille, Ana-Maria Turea, Thibault Cauwenbergh, Jessica Bridoux, Nathalie Lensen, Jessica Mangialetto, Niko van den Brande, Jacinta White, James Gardiner, et al.

Fluorinated peptide hydrogels result in longer *in vivo* residence time after subcutaneous administration

Aurélie Honfroy[1,2,3,4], Jolien Bertouille[1], Ana-Maria Turea[1], Thibault Cauwenbergh[1], Jessica Bridoux[2], Nathalie Lensen[3,4], Jessica Mangialetto,[5] Niko Van den Brande,[5] Jacinta F. White,[6] James Gardiner,[6] Thierry Brigaud[3,4], Steven Ballet[1], Sophie Hernot[2]*, Grégory Chaume[3,4]*, Charlotte Martin[1]*.*

[1] Research Group of Organic Chemistry (ORGC), Vrije Universiteit Brussel, Pleinlaan 2, B-1050 Brussels, Belgium.

[2] VUB, Molecular Imaging and Therapy Research Group (MITH), Laarbeeklaan 103, 1090 Jette, Belgium.

[3] CY Cergy Paris Université, CNRS, BioCIS UMR 8076, 95000 Cergy-Pontoise, France.

[4] Université Paris-Saclay, CNRS, BioCIS UMR 8076, 91400 Orsay, France.

[5] Research group Sustainable Materials Engineering (SUME), lab of Physical Chemistry and Polymer Science (FYSC), Vrije Universiteit Brussel, Pleinlaan 2, B-1050 Brussels, Belgium.

[6] CSIRO Manufacturing, Bayview Avenue, Clayton, VIC 3169, Australia.

Key words: Fluorinated amino acids, peptide hydrogels, mechanical properties, *in vivo* imaging, subcutaneous administration, controlled drug-release.

ABSTRACT

Peptide-based hydrogels are of emerging interest in pharmaceutical and biomedical applications, and the incorporation of fluorinated groups into peptides can confer multiple advantageous properties for the fine-tuning of hydrogel's physicochemical properties. Herein, we have explored the introduction of different fluorinated amino acids in our lead hydrogelator H-FQFQFK-NH_2 (**P1**) to design a series of new fluorinated peptide hydrogels and evaluate the *in vitro* and *in vivo* properties of the most promising analogues. This enables the investigation of the impact of fluorinated groups on peptide gelation, secondary structure and self-assembly processes occurring in the resulting hydrogel systems. We show that the incorporation of fluorine improves the hydrogel stiffness by a factor of 18 compared to the non-fluorinated reference **P1**. Of the three most promising fluorinated analogues **P15** (H-FQFQF(*o*-CF_3)K-NH_2), **P18** (H-FQFQF(F_5)K-NH_2) and **P19** (H-FQFQM(CF_3)K-NH_2), microscopy studies using Transmission Electron Microscopy (TEM) and Atomic Force Microscopy (AFM) demonstrated the impact of fluorine on both fiber morphologies and the alignment in the nanofibrous network. *In vitro* release studies of hydrogels loaded with an opioid cargo suggested an improved hydrogel stability for systems **P15** and **P18**, with less than 5% of the hydrogelator released into the medium after 3 days. This improved stability was further validated *in vivo,* notably with hydrogel **P15** giving the most significant increased gel residence time *in situ*, with more than 20% of hydrogel still present 9 days post-injection, as monitored by nuclear SPECT-CT imaging. Altogether, introducing fluorinated groups in hydrogelator peptide can provide advantageous material properties to form improved hydrogels with longer residence time with extended drug-release potential.

GRAPHICAL ABSTRACT

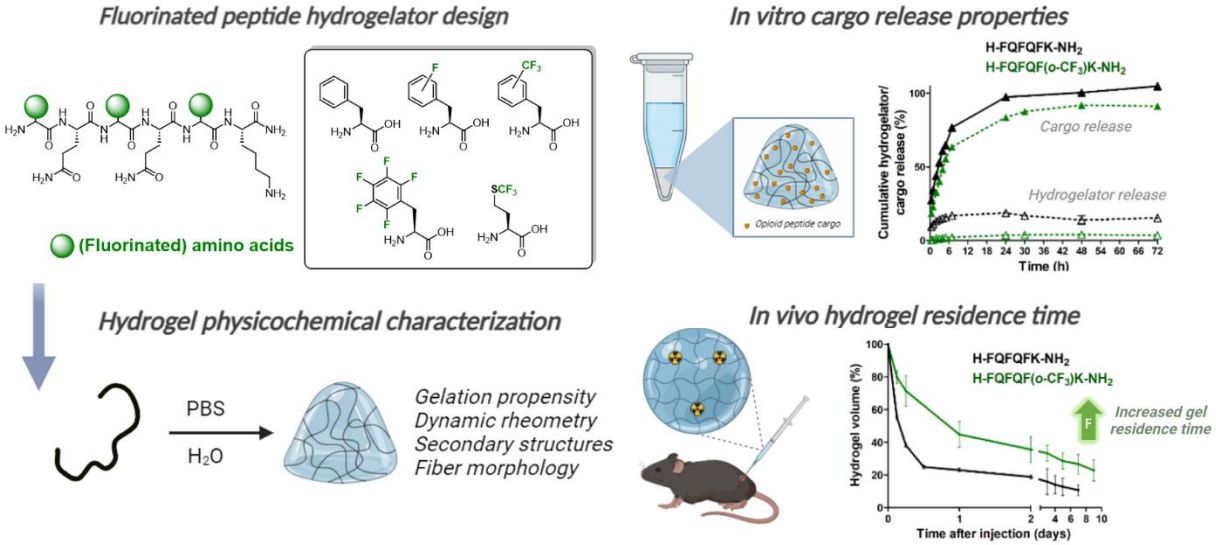

INTRODUCTION

The development of custom drug delivery systems has garnered increased interest from the pharmaceutical community. These provide scaffolds for the enzymatic protection of therapeutics, a reduced dosage of administrated drugs during treatment, as well as a decreased risk of adverse effects.[1–3] Extended release offers many benefits when compared to traditional 'immediate release' administration, presenting a more consistent, prolonged and stabilized drug concentration in plasma. Various routes have been explored for extended drug release.[4] Among them, oral administration is attractive due to its simplicity and non-invasiveness, but it presents a limited duration of action window due to a limited residence time, relatively quick absorption, excretion, the first-pass metabolism step etc, which, taken together, limit drug bioavailability.[5] In contrast, the transdermal route can maintain a longer period of action yet it is often limited by the physicochemical properties of the drug, even though solutions such as microneedles can circumvent this issue,[6] while parental administrations (e.g. subcutaneous and intravenous) might require implants or catheters, exposing the patient to a potential risk of infection. [7–9] Hence, multiple carrier formulations were proposed to meet the specific requirements and overcome the challenge of each administration mode. Among the available extended-release systems, the use of copolymers or nanoparticles (based on dendrimers, micelles, liposomes, nanotubes or magnetic materials), and also hydrogels has been widely reported.[10–13]

Hydrogels in particular have demonstrated their utility in different application domains such as tissue engineering and wound healing, but also sustained drug delivery.[14,15] They represent functional materials build-up of low-molecular-weight molecules that can immobilize water at low concentrations to form three-dimensional networks.[16–19] Interestingly, they are soft materials that present thixotropic behavior, allowing their subcutaneous injectability.[20] Unlike chemical

hydrogels consisting of networks connected by irreversible covalent interactions, physical hydrogels can self-assemble thanks to non-covalent interactions such as ionic bonding, hydrogen bonding, van der Waals interactions or π-stacking interactions.[19,21,22] Among the different types of hydrogels, self-assembling peptides are of particular interest and have received great attention in the last few decades.[23] When compared to polymeric scaffolds, an intrinsic advantage of peptides lies in their biocompatibility and biodegradability.[24,25] Moreover, peptides can be synthesized in a reproducible and controlled manner and the structures can be easily designed to self-organize into various forms by modifying the amino acid sequence. Notably, amphipathic peptides (possessing alternating hydrophobic and hydrophilic amino acids) can assemble into one-dimensional secondary structure, notably β-sheet aggregates that will, after nanofiber entanglement, form a fibrillar three-dimensional hydrogel matrix. [26–28] In 1993, Zhang *et al.* designed the first reported amphipathic peptide capable of forming a hydrogel. It consisted of a 16-mer peptide made up of alternating Ala residues and Glu or Lys amino acids, that folded into β-sheets in phosphate buffered saline (PBS) solution.[29] Using this sequence as a baseline, several groups reported smaller peptide hydrogelators all the while demonstrating the importance of aromatic residues in order to access strong hydrogels.[30,31]

More recently, we developed a set of short injectable amphipathic peptide hydrogels, notably the non-cytotoxic H-FQFQFK-NH_2 peptide (**Figure 1A**).[32,33] *In vivo* application of the hydrogel co-formulated with drugs (e.g. morphine and opioid peptides) demonstrated its effectiveness when injected in mice. The release profile of various loaded drugs could be assessed, giving way to an antinociceptive efficiency recorded up to 4 days and a release time window currently limited to approximately 2 days.[32,34] More recently, we also demonstrated that the use of halogen atoms, in different positions of the hydrogelator sequence could influence the π-π interactions and thus lead

to mechanically stronger gels, particularly when the halogen was incorporated at the fifth position of the sequence (**Figure 1B**).[35]

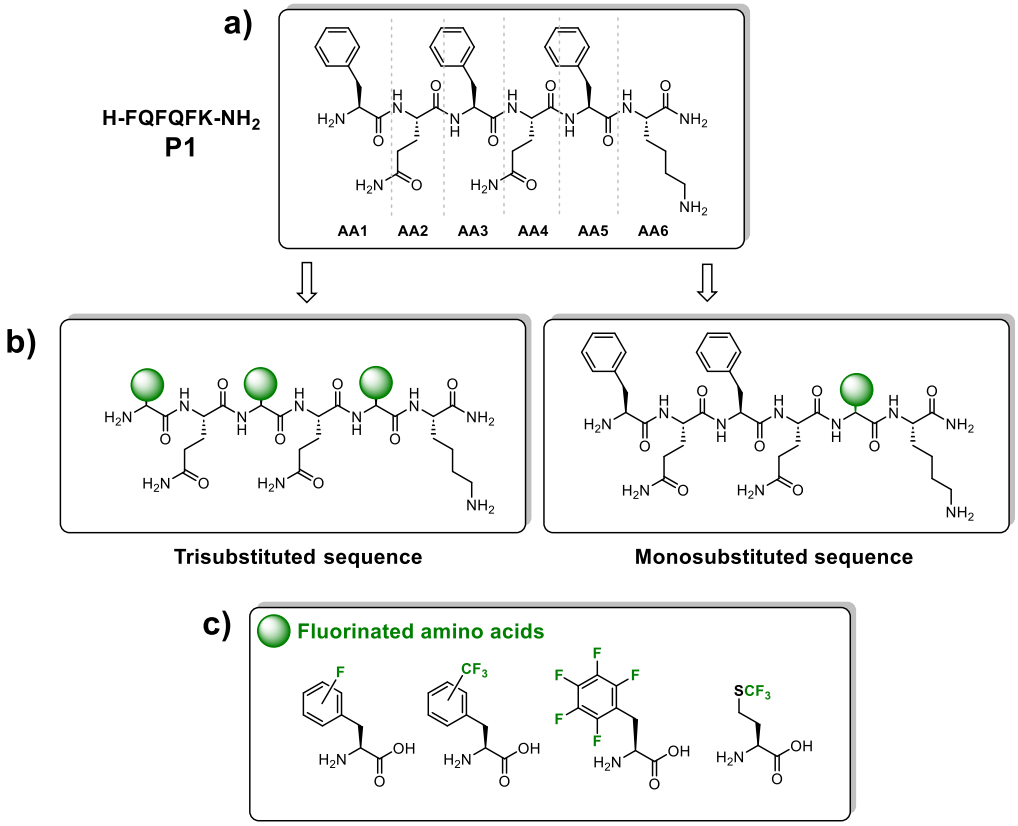

Figure 1. (a) Chemical structure of the non-fluorinated reference hexapeptide hydrogelator **P1**. (b) Fluorine incorporation: Trisubstituted sequence design *versus* monosubstituted sequence. (c) Fluorinated amino acids introduced in the sequence.

The emergence of fluorine in medicinal chemistry has considerably impacted drug design over recent decades, highlighting the potential of fluorine atoms or fluorinated groups when introduced into biomolecules or peptides.[36–40] Indeed, fluorine incorporation permits significant fine-tuning of the physicochemical and biological properties, notably by increasing the lipophilicity[41,42] and, therefore, the lipidic membrane affinity.[43] Fluorine can also induce an increased metabolic stability against proteases[44,45]and it can serve as a probe for ^{19}F NMR, for the investigation of biological

processes.[46–48] Furthermore, fluorinated amino acids have shown their utility in the promotion and stabilization of well-defined secondary structures (i.e., use as a conformational constraint), and self-assembly properties,[49–57] as well as enhancing the biological profile of drug candidates.[38,58,59] Few studies have reported the use of fluorine in the design of hydrogels. Nilsson *et al.* were the first to describe the effect of fluorine on supramolecular hydrogelation with Fmoc-based hydrogelators, and several groups worked on different peptides bearing fluorinated Phe derivatives.[60–64] Their results highlighted the interest of introducing fluorine to accelerate the gelation process kinetics, to increase gel stiffness, and formation of enhanced entangled fiber matrices. However, Fmoc degradation leads to by-products that have shown to induce cytotoxicity.[65] Other systems replacing the Fmoc group were investigated, notably using *N*-1-naphthalene capping (1-Nap)[66], *N*-fluorobenzyl capping[67–69] or more recently, *N*-Boc capping of fluorinated peptide hydrogelators.[70] These studies showed that the increase of fluorine content increases gels stiffness, however, such *N*-capped systems often present weaker mechanical properties, or requires low pH conditions or organic solvent to induce gelation. Hydrogelators incorporating aliphatic fluorinated amino acids were also tested by Koksch *et al*., and showed hydrophobicity increase which could promote β-sheet formation, thus providing better hydrogel formation at physiological conditions.[49]

This work aims at investigating the influence of fluorine introduction into our previously published lead hydrogelator H-$F^1Q^2F^3Q^4F^5K^6$-NH_2 **P1**, in view of improving the hydrogelator in terms of its physicochemical properties and drug release ability. We hypothesize that the introduction of fluorine would increase the local hydrophobicity in the sequence, helping the structuration into β-sheets,[71] to form hydrogels with stronger mechanical properties. We also expect to attain enhanced stability of the hydrogelators *in vivo* using non-proteogenic amino-acids,

potentially prolonging the lifetime of the assembled hydrogel state *in situ* and slow down its erosion process. There is a subtle balance between steric and electronic effects in π–π interactions during self-assembly, and most likely, a complex interplay of the two effects accounts for the observed self-assembly patterns.

More specifically, this work focuses on the introduction of different fluorinated groups along the hydrophobic face of the lead hydrogelator **P1**. Two peptide series were investigated, where only one phenylalanine residue or all three (**Figure 1B**) have been replaced with fluorinated analogues (**Figure 1C**). Gelation propensity was assessed and characterization of the resulting hydrogels was performed by examination of the mechanical properties (dynamic rheometry) and network structuration (circular dichroism, FTIR, AFM and CryoTEM). Moreover, *in vitro* release properties of some fluorinated systems were estimated before the final assessment of their stability *in vivo* using SPECT/CT imaging.

MATERIALS AND METHODS

2.1. Peptide synthesis and purification

All peptides were synthetized using Fmoc-based solid phase synthesis (SPPS), either manually or using an automated peptide synthesizer (Activo-P11, Activotec, Cambridge, UK). Rink amide AM resin (100-200 mesh, 0.64mmol/g) was used as solid support to obtain *C*-terminal peptide amides. Amino acids (3 equiv.) were coupled using *O*-(benzotriazole-1-yl)-*N,N,N′,N′*-tetramethyluronium hexafluorophosphate (HBTU, 3 equiv.) and *N,N*-diisopropylethylamine (DIPEA, 5 equiv.) in dimethylformamide (DMF) for 40 min at room temperature. Fluorinated amino acids were coupled using 2 equivalents. DOTA-substituted peptides were synthesized following the same procedure and by activating DOTA-tris-(*tert*-butyl ester) (1.5 equiv.) with

reagents HBTU (1.5 equiv.) and DIPEA (5 equiv.), in DMF, followed by an overnight coupling at room temperature. Fmoc removal was performed using 4-methylpiperidine in DMF (20:80% v/v) 2 times (for 5 and 15 min). The resin was washed three times with DMF and three times with dichloromethane (DCM). To monitor the coupling reactions, Kaiser tests were performed after each coupling in the case of manual synthesis. After completion of the peptide sequence, peptides were cleaved from the resin with concomitant protecting groups removal using a cleavage cocktail consisting of trifluoroacetic acid (TFA), triisopropylsilane (TIPS), and H_2O (95:2.5:2.5% v/v/v) at room temperature, twice (for 1 h and 3 h, respectively) or for 6 h in the case of DOTA-substituted peptides. After filtration, the solvent was evaporated *in vacuo* and the crude peptide was precipitated in diethyl ether. The residue was then resuspended in H_2O/acetonitrile (ACN) (50:50% v/v) and lyophilized. Crude peptides were dissolved in dimethyl sulfoxide (DMSO) and purified by preparative reverse phase high performance liquid chromatography (RP-HPLC). Pure fractions were combined and lyophilized to yield the pure peptide as a white powder. Purities superior to 95% were assessed by HPLC and high-resolution mass spectrometry (HRMS).

2.2. ^{111}In-labelling of DOTA-labelled peptides for SPECT/CT imaging.

The labelling of DOTA-substituted peptides was performed using different incubation conditions. For hydrogel **P20/P15**, 1 mg DOTA-substituted peptide **P20** was dissolved in ammonium acetate buffer (NH_4OAc) (300 µL, 0.2 M, pH 5), 30 µL of $^{111}InCl_3$ (20 MBq, Curium) was added and the mixture was incubated for 1 h 30 min at 37°C. For hydrogel **P21/P18**, 1 mg DOTA-substituted peptide **P21** was dissolved in ammonium acetate buffer (NH_4OAc) (200 µL, 0.06 M, pH 6.3), 80 µL of $^{111}InCl_3$ (70 MBq) was added and the mixture was incubated for 2 h at 37°C. For hydrogel **P22/P19**, 1 mg DOTA-substituted peptide **P22** was dissolved in ammonium

acetate buffer (NH_4OAc) (200 µL, 0.1 M, pH 6), 80 µL of $^{111}InCl_3$ (71 MBq) was added and the mixture was incubated for 2 h at 37°C. For each mixture, a purification on a tC18 cartridge (Sep-Pak Vac 1cc, Waters) (elution with acetonitrile) was performed and the radiochemical purity (>95%) was validated through the pure fraction of ^{111}In-labelled hydrogelator obtained by instant thin layer chromatography (ITLC), using sodium citrate buffer (0.1 M, pH 5) as mobile phase. The acetonitrile solvent was evaporated under nitrogen flow prior to hydrogel preparation.

2.3. Hydrogel preparation

2.3.1. For gelation tests, pH measurements and CD experiments.

Peptide gelation was performed by dissolving 2 mg of hydrogelator (2% w/v; as TFA salt) in 100 µL of phosphate-buffered saline (PBS) solution (pH 7.4) in an Eppendorf® tube. After being vortexed for 1 min, centrifugated for 2 min and sonicated for 15 min (the three steps are repeated three times), the gel is left to rest overnight at room temperature. The gelation capacity of each fluorinated peptide was assessed qualitatively using the inverted tube test. A successful gelation was characterized by the absence of gravitational flow after inverting the Eppendorf® tube.[32]

2.3.2. For *in vitro* cargo release

Stock solutions of the cargo H-Dmt-D-Arg-Phe-Phe-NH_2 **C1** were first made in PBS solution at a concentration of 2.2 mg/mL (0.22% w/v). Gelation was achieved by adding 100 µL of this stock solution to 2 mg of hydrogelator (2% w/v; as TFA salt) in an Eppendorf® tube. After being vortexed for 1 min, centrifugated for 2 min and sonicated for 15 min (the three steps are repeated three times), the gel was left to rest overnight at room temperature.

2.3.3. For dynamic rheometry

The peptide gelation was performed by dissolving 20 mg of hydrogelator (2% w/v, as TFA salt) in 1 mL of PBS solution (pH 7.4) in a 2 mL syringe closed with a cap and a piston. After being vortexed for 1 min, centrifugated for 2 min and sonicated for 15 min (the three steps are repeated three times), the gel is left to rest overnight at room temperature in the syringe.

2.3.4. For transmission electron microscopy and atomic force microscopy

The peptide gelation was performed by dissolving 0.1 or 2 mg of the hydrogelator (0.1% w/v and 2% w/v, respectively, as TFA salt) in 100 µL of PBS (pH 7.4) in an Eppendorf® tube. After being vortexed for 1 min, centrifugated for 2 min and sonicated for 15 min (the three steps are repeated three times), the gel is left to rest overnight at room temperature.

2.3.5. For *in vivo* gel stability

The formation of the ^{111}In-labelled hydrogel was conducted by the addition of PBS on the ^{111}In-labelled hydrogelator described above (see section 2.2) until a volume of 1 mL is obtained. To initiate the gelation, 20 mg of non-labelled hydrogelator was weighted in a 5 mL Eppendorf® and the ^{111}In-labelled solution in PBS was added to form the 2% w/v hydrogel. After three repetitive steps of 1 min vortexing and 15 min sonication, the gel was left to rest overnight at room temperature.

2.4. RP-HPLC assay for estimation of hydrophobicity

RP-HPLC was performed on a Chromaster VWR HITACHI, equipped with a Chromaster HPLC 5430 Diode Array UV detector, a Chromaster HPLC 5310 Column Oven, a Chromaster HPLC 5260 Auto Sampler and a Chromaster HPLC 5160 Pump. The column used for analysis was a Chromolith® High Resolution C18 endcapped column (50 mm x 4.6 mm, 1.1 µm, 150 Å). The

samples were monitored by UV absorbance at a detection wavelength of 214 nm. The utilized flow rate was 2.8 mL/min, with a 6 min run time. The eluent used was a mixture of H_2O (A) and ACN (B), both acidified with 0.1% TFA, with a linear gradient of 1% to 100% B.

2.5. Dynamic rheometry

Dynamic rheometry experiments were conducted on a Discovery HR-2 hybrid rheometer from TA Instruments equipped with a 40 mm Peltier plate and a Peltier Solvent trap containing Evaporation Blocker accessories. Temperature stability was enabled by water cooling while mineral oil was used in the well to avoid solvent evaporation. Hydrogel samples were prepared (as described in section 2.3.3) and injected through a 21 G needle, after overnight curing, between the rheometer plates thereby keeping the gap size as low as possible to minimize solvent evaporation. The measurements were performed with a gap of 500 μm over 2 h of time sweep at 0.15 Hz frequency and 0.5% strain at 37°C. Experiments were conducted in triplicate and data presented as mean values ± standard deviation (SD).

2.6. CD experiments

CD spectra were recorded using a BioLogic MOS-500 spectrometer, running on Biokine V4.80 software. Measurements were performed at 20°C, with 3 scans per measurement, a scan rate of 50 nm/min, 2.0 nm bandwidth, at a 0.5 nm resolution. Data are measured at wavelengths between 190 nm and 260 nm (Xe lamp). Samples were prepared as described in section 2.3.1 and approximately 20 μL were directly applied to a quartz cell window cuvette (Hellma, 106-0.01-40, path length l = 0.01 mm) held by a holder (Hellma, 013-000-71). The background spectrum was subtracted from each sample spectrum.

2.7. Negative stain transmission electron microscopy

Carbon film coated copper grids (ProSciTech, EMSCF200H-Cu-TH for the 0.1% w/v solution and EMSCF 300H-Cu-TH for the 2% w/v gels) were ionized with Pelco easiGlow to make them hydrophilic and held in anti-capillary forceps. Samples were prepared as described in section 2.3.4. For the 0.1% w/v samples, ~2 µL was applied on the grids with a pipet, for the 2% w/v samples, a small gel aliquot was applied on the grid with a spatula. The material adsorbed for ~60 s in a moistened environment and excess material was wicked away with filter paper (Whatman 541). The grid was inverted onto a 30 µL drop of 2 % phosphotungstic acid (PTA) stain (pH 6.9) on Parafilm for ~10 s. The excess of stain was wicked away with filter paper (Whatman 541) and the grid was air-dried for 30 min or 12 h before imaging.

Transmission electron microscopy (TEM) images were obtained with a Tecnai 12 Transmission Electron Microscope (FEI, Oregon, USA) with operating voltage of 120 kV, equipped with a FEI Eagle 4kx4k CCD camera and AnalySIS v3.2 camera control software (Olympus, Tokyo, Japan). An electron dose of 400-800 electrons/nm2s was applied during imaging and different grid locations were imaged for each sample. Dimensions of the fibers were acquired in the software ImageJ.

2.8. Cryogenic transmission electron microscopy

The samples were made in a laboratory-built vitrification grid plunge system, the humidity was kept close to 80% and ambient temperature was 22°C. 300-Mesh copper grids (ProSciTech, GSCu300FL-50C) coated with lacey formvar over a perforated carbon support were ionized with Pelco easiGlow to make them hydrophilic. Samples were prepared as described in section 2.3.4. For the 0.1% w/v samples, ~2 µL was applied on the grids with a pipet, for the 2% w/v samples, a small gel aliquot was applied on the grid with a spatula. The material adsorbed for ~10 s prior to

manual blotting with filter paper (Whatman 541) for approximately 2 s. Immediately thereafter, the grids were plunged in liquid ethane cooled by liquid nitrogen and the frozen grids were stored in liquid nitrogen until use.

TEM images were obtained with a Tecnai 12 Transmission Electron Microscope (FEI, Oregon, USA) with operating voltage of 120 kV, equipped with a Gatan 626 cryoholder (Gatan, Singapore), a FEI Eagle 4kx4k CCD camera and AnalySIS v3.2 camera control software (Olympus, Tokyo, Japan). A low electron dose of 200-600 electrons/nm^2s was applied during imaging and different grid locations were imaged for each sample.

2.9. Atomic force microscopy

Samples were prepared as described in section 2.3.4. A volume of ~50 μL of the 0.1% w/v solution or the 2% w/v gel was applied on freshly cleaved mica surrounded with Teflon tape. The peptide assemblies adsorbed for 30 min and the excess of material was washed away 3 times with 100 μL PBS. Next, a 200 μL PBS bubble was deposited on the mica.

A JPK Nanowizard ULTRA Speed 2 AFM (Bruker, Germany) in AC fast imaging mode was used for the data recording. The Fastscan-D cantilever, with a nominal spring constant of 0.25 Nm^{-1} and a nominal frequency of 110 kHz, was immersed in the water bubble and images were recorded with a line rate of 10 lines/s, a setpoint in the range of 5-22 nm, an integral gain of 1500 Hz, a proportional gain of 0.02 and a resolution of 512x512 pixels. Different surface locations were scanned for each sample. All images were plane fitted and line levelled using the JPK Data Processing software version 7 (Bruker). Fiber dimensions were measured in the same software.

2.10. *In vitro* release studies

A volume of 500 μL of PBS solution (pH 7.4, 37°C) was added gently on each cargo loaded hydrogel (described above in section 2.3.2) (= timepoint 0). Samples of 10 μL of supernatant were

collected at regular timepoints after a careful homogenization of the solution, before being replaced by 10 µL of fresh PBS solution (37°C). Samples were analyzed by a RP-HPLC system, as described below. The cumulative dose released *Mt* (µg) was calculated over time using the area under the curve (AUC) values and calibration curves of the cargo stock solution and of the peptide hydrogelator stock solutions. Then, the cumulative release percentage was determined using **Eq.1**, with *Mi* being the initial encapsulated cargo dose. Data were then plotted for each formulation. Experiments were conducted in triplicate and data presented as mean values ± SD.

$$\%\text{Cumulative cargo release} = \frac{Mt}{Mi} \times 100 \ (\textbf{Eq. 1})$$

For data analysis of *in vitro* release experiments, an Agilent Technologies 1100 Series system was used. This system contains a G1311A Quaternary Pump, G1379B degasser, G1313A ALS Auto Sampler, a C1316A ColComp column compartment and a variable wavelength detector VWD G1314B (detection wavelength at 214 nm). The column is an EC NUCLEODUR C18 end capped column (150 mm x 2 mm, 5 µm, 300 Å). The eluent was a mixture of solvents H_2O (A) and ACN (B), both acidified with 0.1% TFA. For release experiments on **P1** and **P15**, a gradient of 10% to 60% B was applied over 19 min, followed by a gradient of 60% to 100% B over 2 min. For **P18**, a gradient of 5% to 40% B was applied over 19 min, followed by a gradient of 40% to 100% B over 2 min. For **P19**, a gradient of 5% to 34% B was applied from 0 to 23 min, followed by a gradient of 34% to 100% B for 2 min. The flow rate used was 0.3 mL/min, with a run time of 30 min.

2.11. *In vivo* hydrogel stability by SPECT/CT imaging.

Protocols were approved by the Ethics Committee for Animal Experiments of the Vrije Universiteit Brussels (project number 23-272-19) and subjected to the provisions of the Royal Decree of 29 May 2013 concerning the protection of animals used for scientific purposes and the

Regulations of the Ethics Committee for Animal Experiments. Female C57BL/6 J mice (from Charles River, L'Abresle, France) were used, with 3 mice per group. The mice were housed in individually ventilated cages at 19–24°C in 40–60% humidity with a light/dark cycle of 14/10 h. Food pellets and water were provided *ad libitum*. Before the start of the experiment, the mice were acclimatized to the new environment for at least one week. All experimental procedures were performed under 2–5% isoflurane anesthesia, with an oxygen flow rate of 0.5–1.5 L/min. Body condition score, animal behavior and physical appearance were daily checked. At the end of the study, mice were killed by cervical dislocation.

A volume of approximately 150 µL of the 2% w/v hydrogel loaded with ^{111}In-labelled hydrogelator (see preparation in section 2.3.5.) (0.099–1.407 MBq) was injected subcutaneously, just above the right hind limb of the mice. Animals were then subjected to non-invasive SPECT/CT scans at different time-points post-injection (0 h, 3 h, 6 h, 24 h, 2 days, 3 days, 4 days, 5 days, 6 days, 7 days, 8 days and 9 days depending on the formulation, with a maximum total number of 10 scans per mice). SPECT/CT imaging was performed on a Vector+ system (MiLabs) equipped with a general-purpose rat/mouse 1.5 mm 75 pinhole collimator. Scans were performed in spiral mode with 6 bed positions and an acquisition time of 200 s per bed position. For image reconstruction, 2 subsets and 4 iterations were used, with a voxel size of 0.4 mm, in U-SPECT-Rec software (Milabs). The CT scan was made in 1 bed position, with a duration of 146 s at 60 kV and a pixel size of 80 µm. The acquired images were processed and quantified using the AMIDE software. More specifically, all images were equally scaled (0–1500% ID/cc) and a region of interest (ROI) was drawn around the injection site of the hydrogel. The total radioactivity within this ROI was then calculated and expressed as percentage of injected dose (% ID/cc) remaining as

a function of time. All data were presented as mean values ± SD. 3D volume rendering images were prepared in AMIDE software.

RESULTS AND DISCUSSION

3.1. Peptide design and synthesis

Among the properties conferred by the introduction of fluorine atoms or fluorinated groups, it is known that their incorporation into aromatic ring alter its electronic distribution, impacting the interactions of the arenes with their environment, as illustrated in **Figure 2**.[72]

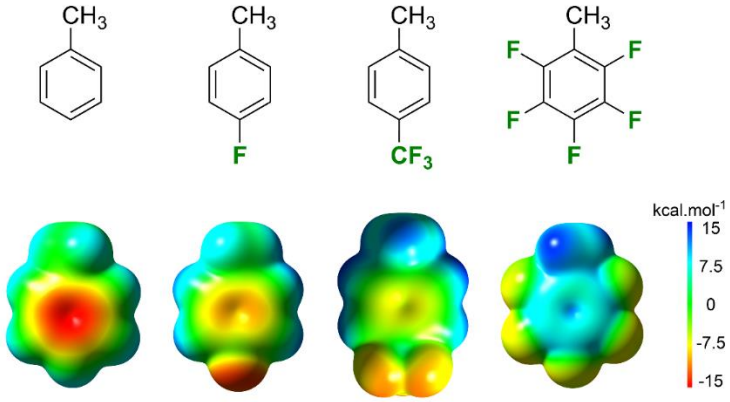

Figure 2. Electrostatic potential map (Isovalue: 0.001 e/au^3) of toluene and fluorinated derivatives, calculated with GaussView 6 from optimized structure at the B-3LYP/6-31G(d) level of theory without any solvent correction. Calculation based on Wheeler and Houk method.[73]

In this work, we aim to study the influence of fluorine on the self-assembly properties of hydrogel sequence **P1**, taking into consideration the Hansch-Leo parameter π, a value that ranks the lipophilicity of a benzene substituent.[74,75] Different fluorinated amino acids were selected, including phenylalanine analogues bearing one fluorine substituent, a CF_3 group, as well as the pentasubstituted phenylalanine (Phe(F_5)). This selection was made in order to have a gradation in hydrophobicity, since it has been reported that the trifluoromethyl group displays higher

lipophilicity than the fluorine atom alone (Hansch-Leo parameter π_x (CF_3) = +0.88, π_x (F) = +0.14).[74,75] Additionally, we introduce these different substituents on different positions of the aromatic ring (*ortho*, *meta*, *para*). Next to the fluorinated phenylalanine analogues, we decided to evaluate the importance of aromaticity versus hydrophobicity introducing the modified amino acid trifluoromethionine. Interestingly, this last amino acid has shown to induce outstanding hydrophobicity in peptides.[41]

Our design is based on the systematic substitution of one or all Phe residues of the hydrophobic face of the amphipathic sequence, by (non)aromatic fluorinated analogues. Importantly, for the monosubstituted sequences, only the 5th position has been considered since previous work demonstrated that incorporation of a halogen atom at this position of the hexamer sequence resulted in the highest improvement of mechanical properties, as determined by rheological experiments.[35] To this end, starting from the lead sequence H-FQFQFK-NH_2 (**P1**), two series of fluorinated hexapeptide hydrogelators (**Table 1**) were successfully synthesized by standard Fmoc SPPS strategy. Peptides have been obtained in good yields (between 14 and 68%) and high purity (> 95%). The first series involved the replacement of the three phenylalanine residues in **P1** by different fluorinated amino acids (providing **P4-P11**), while the second series contained a single amino acid substitution on the 5th position (providing **P12-P19**). Next to these fluorinated hydrogelators, two non-fluorinated peptide references containing methionine (Met) residues have also been prepared (**P2** and **P3**), to better assess the influence of fluorine on the physicochemical and mechanical properties of the hydrogels when incorporated as a Met(CF_3) (non-fluorinated analogues of **P11** and **P19**, respectively).

In a previous study, we demonstrated that when introduced on the aryl ring of Phe, the fluorine atom induces a less stabilizing effect for stacking interactions, as compared to another halogen.[35]

Nonetheless, most of the resulting fluorinated hexapeptide hydrogels of that study, still presented higher storage moduli values (*G'*) compared to the non-halogenated reference hydrogel **P1**, hence confirming an increased hydrogel rigidity.[35] So far, only hydrogelators bearing one or two Phe(*m*F) residue were described. Therefore, the first modification that we considered consisted of the systematic introduction of a single fluorine atom on each phenylalanine of the sequence, in *ortho*, *meta* or *para* position of the phenyl ring (giving respectively **P4**, **P5** and **P6**). Then, following the same approach, peptides bearing a trifluoromethyl (-CF_3) group in the *ortho*, *meta* and *para* position of the aryl ring have been prepared, yielding **P7**, **P8** and **P9,** respectively. **P10** was synthesized by introducing pentafluoro-phenylalanine on the three amino acid positions within the peptide sequence. To evaluate the importance of the aromaticity of the phenyl ring relatively to the lateral chain hydrophobicity in general, we also included peptide **P11**, which bears Met(CF_3) instead of Phe residues, an amino acid that was previously reported to introduce high hydrophobicity, when incorporated into peptides.[41] Finally, peptides **P12**-**P19** were synthesized as monosubstituted analogues of peptides **P4**-**P11**, respectively.

Table 1. Overview of the different hydrogelators synthesized in this work.

Code	Internal SBL code	Peptide sequence	Rt (min)[a]	Gelation[b]	Aspect
Non-fluorinated references					
P1	**SBL-HG-063**	H-Phe-Gln-Phe-Gln-Phe-Lys-NH_2	2.72	Yes	Transparent
P2	**SBL-HG-248**	H-Met-Gln-Met-Gln-Met-Lys-NH_2	2.17	No	NA
P3	**SBL-HG-301**	H-Phe-Gln-Phe-Gln-Met-Lys-NH_2	2.50	Yes	Transparent
Trisubstituted hexapeptides					
P4	**SBL-HG-215**	H-Phe(*o*F)-Gln-Phe(*o*F)-Gln-Phe(*o*F)-Lys-NH_2	2.76	Yes	Transparent
P5	**SBL-HG-216**	H-Phe(*m*F)-Gln-Phe(*m*F)-Gln-Phe(*m*F)-Lys-NH_2	2.81	Yes	Transparent
P6	**SBL-HG-217**	H-Phe(*p*F)-Gln-Phe(*p*F)-Gln-Phe(*p*F)-Lys-NH_2	2.83	Yes	Transparent
P7	**SBL-HG-218**	H-Phe(*o*CF_3)-Gln-Phe(*o*CF_3)-Gln-Phe(*o*CF_3)-Lys-NH_2	3.20	Yes	Opaque
P8	**SBL-HG-219**	H-Phe(*m*CF_3)-Gln-Phe(*m*CF_3)-Gln-Phe(*m*CF_3)-Lys-NH_2	3.31	Yes	Opaque
P9	**SBL-HG-220**	H-Phe(*p*CF_3)-Gln-Phe(*p*CF_3)-Gln-Phe(*p*CF_3)-Lys-NH_2	3.27	Yes	Opaque
P10	**SBL-HG-221**	H-Phe(F_5)-Gln-Phe(F_5)-Gln-Phe(F_5)-Lys-NH_2	3.18	Yes	Opaque
P11	**SBL-HG-222**	H-Met(CF_3)-Gln-Met(CF_3)-Gln-Met(CF_3)-Lys-NH_2	2.95	Yes	Transparent
Monosubstituted hexapeptides					
P12	**SBL-HG-316**	H-Phe-Gln-Phe-Gln-Phe(*o*F)-Lys-NH_2	2.69	Yes	Transparent
P13	**SBL-HG-166**	H-Phe-Gln-Phe-Gln-Phe(*m*F)-Lys-NH_2	2.68	Yes	Transparent
P14	**SBL-HG-317**	H-Phe-Gln-Phe-Gln-Phe(*p*F)-Lys-NH_2	2.70	Yes	Transparent
P15	**SBL-HG-236**	H-Phe-Gln-Phe-Gln-Phe(*o*CF_3)-Lys-NH_2	2.88	Yes	Transparent
P16	**SBL-HG-223**	H-Phe-Gln-Phe-Gln-Phe(*m*CF_3)-Lys-NH_2	2.94	Yes	Transparent
P17	**SBL-HG-224**	H-Phe-Gln-Phe-Gln-Phe(*p*CF_3)-Lys-NH_2	2.97	Yes	Transparent
P18	**SBL-HG-237**	H-Phe-Gln-Phe-Gln-Phe(F_5)-Lys-NH_2	2.87	Yes	Transparent
P19	**SBL-HG-225**	H-Phe-Gln-Phe-Gln-Met(CF_3)-Lys-NH_2	2.76	Yes	Transparent
DOTA-labelled peptide hydrogelators for SPECT/CT imaging					
P20	**SBL-HG-318**	DOTA-βAla-Phe-Gln-Phe-Gln-Phe(*o*CF_3)-Lys-NH_2	2.90	-	-
P21	**SBL-HG-319**	DOTA-βAla-Phe-Gln-Phe-Gln-Phe(F_5)-Lys-NH_2	2.91	-	-
P22	**SBL-HG-322**	DOTA-βAla-Phe-Gln-Phe-Gln-Met(CF_3)-Lys-NH_2	2.81	-	-

[a] Peptide retention time (Rt) in min, determined by RP-HPLC; [b] Gelation assessment based on the inverted tube test.

3.2. Assessment of the hydrophobicity

First, the hydrophobicity character of each peptide was assessed by determining their retention time in reversed phase HPLC analyses. As expected, all synthesized fluorinated analogues displayed higher retention times compared to the corresponding non-fluorinated reference sequence **P1 (Table 1 & Figure 3)**. Moreover, the retention time increased even more for peptides containing three -CF_3 groups (between 3.20-3.31 min) compared to peptides bearing a single fluorine atom (2.68-2.70 min; **Table 1** & **Figure 3** bottom). Additionally, the retention times also seemed to be related to the position of the fluorinated substituents on the aryl ring and mostly tended to increase following the order *ortho*<*meta*<*para*. Consequently, an increase in fluorine content in peptides could be partially correlated to the overall increase in hydrophobicity of the fluorinated peptides, as shown by increased retention times. The correlation did not fully stand, as the pentafluoro-phenylalanine analogues were characterized by a slightly lower retention time, as compared to the trifluoromethylated ones (**Table 1** and **Figure 3**).

3.3. Gelation properties

The gelation properties of each peptide were qualitatively determined through the use of the inverted-tube test at 2% w/v (**Figure 3**). This concentration matches that previously used for the reference sequence **P1)**.[34] This test has been used to screen the gelation ability as well as the physical appearance of each hydrogel prior to further characterization. According to this visual test, most peptides were able to form gels in PBS. In the case of trisubstituted peptides, analogues bearing Phe(*o/m/p*-F) (**P4-P6**) were able to form transparent gels at 2%w/v. Interestingly, these results contrast with our previous study where peptides bearing three halogenated Phe's (Phe(*p*I), Phe(*p*Cl) or Phe(*p*Br)) were not able to form gels. Here, peptide **P6**, bearing three Phe(*p*F), presents a surprising hydrogelation capacity that does not follow the trend previously observed with other

halogen atoms. This observation might be related to an electronic effect of fluorine in the system.[50] Indeed, fluorine is known to highly polarize aromatic rings by increasing the electronic density in its surrounding and decreasing the electron density of the aromatic ring. An alternative explanation can be based on less steric hindrance of three fluorine atoms during self-assembly, as compared to the larger halogen atoms.

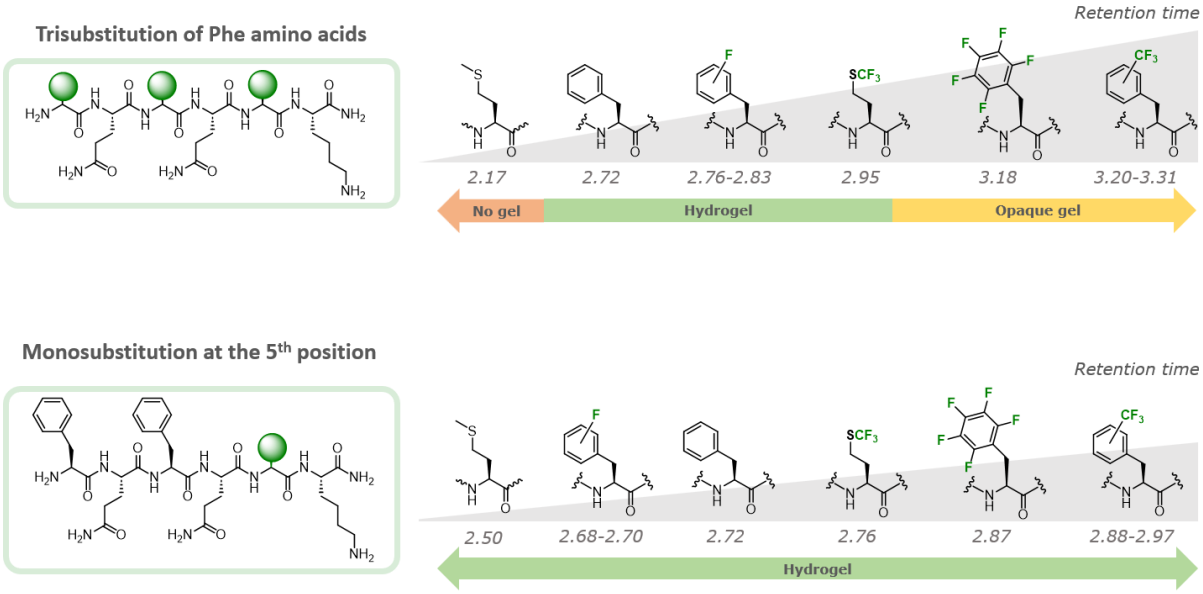

Figure 3. Gelation ability and retention time related to amino acid structure of the modified sites. In the case of *ortho/meta/para* isomers, a range of retention times is given.

The Hammett constant of fluorine in *para* position of the ring was lower than for other halogen substituents ($\sigma_p(F) = 0.06$; $\sigma_p(Br) = 0.23$; $\sigma_p(Cl) = 0.23$; $\sigma_p(I) = 0.28$), suggesting a lower influence of fluorine on charge distribution, thus potentially inducing less changes for structuration and thus gelation capacity.[75] Nilsson *et al.* already hypothesized the participation of halogen substituents on the more direct strand-strand lamination observed in Fmoc-4-X-Phe hydrogels (with X = F, Br, Cl and I).[61] In contrast, the series of analogues bearing Phe(*o/m/p*-CF_3) (**P7-P9**) led to opaque gels, suggesting a lowered peptide dissolution in the hydrogel. We can hypothesize that the addition of

a trifluoromethyl group on the aryl ring brings bulkiness and electron-deficiency to the ring system, hence altering hydrophobic interactions between neighboring rings, eventually leading to longer center-to-center distances between electron-deficient rings. Moreover, the Hammett constants of a CF_3 group is higher than for a F substituent, suggesting a higher influence on charge distribution ($\sigma_p(CF_3) = 0.54$; $\sigma_m(CF_3) = 0.43$; $\sigma_p(F) = 0.06$; $\sigma_m(F) = 0.34$) (**Figure 2**).[75] Additionally, the hydrophobic character (based on retention times) is increased, leading to lowered peptide dissolution, which might explain the higher opaqueness of the resulting hydrogels **P8** and **P9** *(***Figure 3**). Regarding **P10**, which contains Phe(F_5) residues, it presented an intermediate hydrophobicity (Rt = 3.18 min) between Phe(F) peptides (**P4**-**P6**: Rt = 2.76-2.83 min) and Phe(CF_3) peptides (**P7**-**P9**: Rt = 3.20-3.31 min) analogues. Finally, to evaluate the importance of the aromaticity relative to the hydrophobicity, **P11** bearing Met(CF_3) was prepared, resulting in a transparent gel. However, in the same conditions, its non-fluorinated analogue **P2** didn't form a gel, highlighting the role of the -CF_3 group in efficient gelation, since only **P11** was able to promote gelation. Additionally, it was most noteworthy that when the Phe residues (**P1**) were replaced by Met (**P2**), it significantly affected the rt (2.72 min vs 2.17 min, respectively), while the -CF_3 group could counterbalance that hydrophobicity loss (**P11**: 2.95 min), and led to **P11** gelation. Altogether, these results suggest that the overall hydrophobicity of the peptides is a determinant parameter that dictates the self-assembly properties of amphipathic peptides. Most interestingly, we have demonstrated that fluorine could counterbalance the lack of aromaticity in amphipathic sequences containing only aliphatic residues.

Because we observed that high fluorine content could be detrimental for the transparency of the hydrogels and suggest a (partial) peptide precipitation, we also synthesized a set of monosubstituted versions of the previously discussed peptides (**P12**-**P19)**. As expected, this series

of analogues displayed intermediate hydrophobicity (based on retention times), ranging between the retention times of their corresponding non-fluorinated sequences and of trisubstituted fluorinated analogues. Based on the inverted tube test, all monosubstituted analogues were able to form strong transparent gels at 2% w/v. Therefore, the introduction of a single fluorinated amino acid in the hexapeptide sequence seems to balance the physicochemical properties of the peptide to induce gelation.

In addition to the visual test, the pH of each gel was monitored for *in vivo* considerations (See Supportive Information, **Table S2**). As a result, all hydrogels showed pH values relatively close to the reference **P1**, with most of the lowest values obtained on trisubstituted sequences.

3.4. Characterization of mechanical properties by dynamic rheometry

After screening the gelation properties of each analogue qualitatively, the mechanical properties of all modified hydrogels were quantitatively assessed by dynamic rheometry. It was decided to perform this characterization only on transparent hydrogels, thus discarding peptides **P7-P10** as their opaqueness is indicative of a heterogenous gel. After overnight cure in a syringe, hydrogels were injected between the rheometer plates. Importantly, the injection process can mimic the shear occurring during *in vivo* subcutaneous injection. Of note, different values were recorded during time sweep experiments, including the storage modulus *G',* that describes the elastic properties of the material (or its solid-state behavior), and the loss modulus *G",* which describes the viscous properties of the material (or its liquid-state behavior). The hydrogel state can be confirmed when G' is superior to G".[76] The phase angle δ (that defines a dominant elastic behavior when close to 0° and a dominant viscous behavior when close to 90°) is reported in the supplementary data *(***Figures S4-S17**).

Table 2. Overview of the storage moduli *(G')* and loss moduli (*G''*) ± SD, recorded using dynamic rheometry on 2% w/v gels in PBS. All reported values have been extracted from the end of the 2 h time sweep.

Code	Peptide sequence	Storage modulus G' (Pa)	Loss modulus G'' (Pa)
Non-fluorinated references			
P1	H-Phe-Gln-Phe-Gln-Phe-Lys-NH_2	1792 ± 236	162 ± 31
P3	H-Phe-Gln-Phe-Gln-Met-Lys-NH_2	2943 ± 1955	227 ± 147
Trisubstituted hexapeptides			
P4	H-Phe(*o*F)-Gln-Phe(*o*F)-Gln-Phe(*o*F)-Lys-NH_2	1562 ± 169	176 ± 31
P5	H-Phe(*m*F)-Gln-Phe(*m*F)-Gln-Phe(*m*F)-Lys-NH_2	2319 ± 583	325 ± 84
P6	H-Phe(*p*F)-Gln-Phe(*p*F)-Gln-Phe(*p*F)-Lys-NH_2	2846 ± 244	318 ± 36
P11	H-Met(CF_3)-Gln-Met(CF_3)-Gln-Met(CF_3)-Lys-NH_2	1642 ± 277	162 ± 42
Monosubstituted hexapeptides			
P12	H-Phe-Gln-Phe-Gln-Phe(*o*F)-Lys-NH_2	5120 ± 3102	1549 ± 1508
P13	H-Phe-Gln-Phe-Gln-Phe(*m*F)-Lys-NH_2	606 ± 316	82 ± 53
P14	H-Phe-Gln-Phe-Gln-Phe(*p*F)-Lys-NH_2	8110 ± 2960	1287 ± 472
P15	H-Phe-Gln-Phe-Gln-Phe(*o*CF_3)-Lys-NH_2	13039 ± 8206	921 ± 319
P16	H-Phe-Gln-Phe-Gln-Phe (*m*CF_3)-Lys-NH_2	9464 ± 4798	1218 ± 575
P17	H-Phe-Gln-Phe-Gln-Phe(*p*CF_3)-Lys-NH_2	5651 ± 399	621 ± 67
P18	H-Phe-Gln-Phe-Gln-Phe(F_5)-Lys-NH_2	16649 ± 1644	1546 ± 205
P19	H-Phe-Gln-Phe-Gln-Met(CF_3)-Lys-NH_2	33876 ± 4949	1354 ± 403

Based on the data in **Table 2**, *G'* is significantly superior to *G'',* confirming the hydrogel state. In order to evaluate the influence of the fluorine content on the mechanical properties of the resulting hydrogels, *G'* values were compared for each system. In general, it appears that the incorporation of fluorinated groups in the sequence allows substantial increase of the storage

modulus *G'* of the hydrogels, as compared to the non-fluorinated reference **P1**. This increase is, however, less obvious in the case of peptides **P4**-**P6**, bearing three monofluorinated phenylalanine residues, since similar rheological profiles and storage moduli in the same order of magnitude were observed, compared to **P1** (**Table 2**). A similar rheological profile as the reference **P1** was obtained for the non-aromatic analogue **P11**, which here again validates the capacity of fluorine to counterbalance the lack of aromaticity and maintaining an ability to gelate.

However, for the analogues bearing only one monofluorinated phenylalanine **P12-P14**, different profiles were obtained. For **P12** and **P14**, respectively bearing a fluorine atom on the *ortho* and *para* position of the 5th Phe, a high *G'* value was obtained after 2 h of experiment. In contrast, for **P13** which bears a fluorine on the *meta* position of the Phe, a lower *G'* value was observed. These results suggest that introducing fluorine in the *meta* position of only one Phe of the sequence destabilizes the hydrogel network, in agreement with the trend previously published on the stabilizing effect of different halogen substituents when located in different positions of a toluene model system.[35] However, this observation contrasts with previous results from Nilsson's group on Fmoc-*n*-F-Phe derivatives, with *meta*-F substituent giving the stiffest gel.

For comparison, the introduction of one trifluoromethylated phenylalanine residue (**P15-P17**), resulted in a significant increase in *G'* ranging from 5651 up to 13039 Pa. Finally, hydrogels **P18** and **P19** displayed the highest storage moduli among the series, being respectively 10 times or >18 times superior to **P1**, respectively. For hydrogels **P15** to **P18**, the fifth phenylalanine ring contains fluorinated groups inducing a strong electron deficiency in the ring. However, it has been shown in literature that neighboring fluorinated and non-fluorinated rings, bearing opposite quadrupolar moments (thus having complementary charged interactions) can undergo a more direct sandwich stacking and packing of the phenyl groups compared to the non-fluorinated analogues together.[67]

As a result, we hypothesized that fluorinated substituents would improve the stacking between the fluorinated ring and their direct neighboring ring. Therefore, a better lamination was expected upon stacking inter-strand Phe derivatives with opposite quadrupole moments. For hydrogel **P19**, the introduction of an aliphatic residue on the 5th position, Met(CF_3), might help the stacking of the strand. We hypothesized that this amino acid is less bulky and sufficiently hydrophobic, leading to a self-assembly into a higher density network. **Figure 4** shows the storage and loss moduli curves of the peptide hydrogels with the highest moduli of the set; **P15**, **P18** and **P19,** in comparison to the reference **P1**. Additional rheological measurements can be found in Supporting information (**Figures S4-S17**).

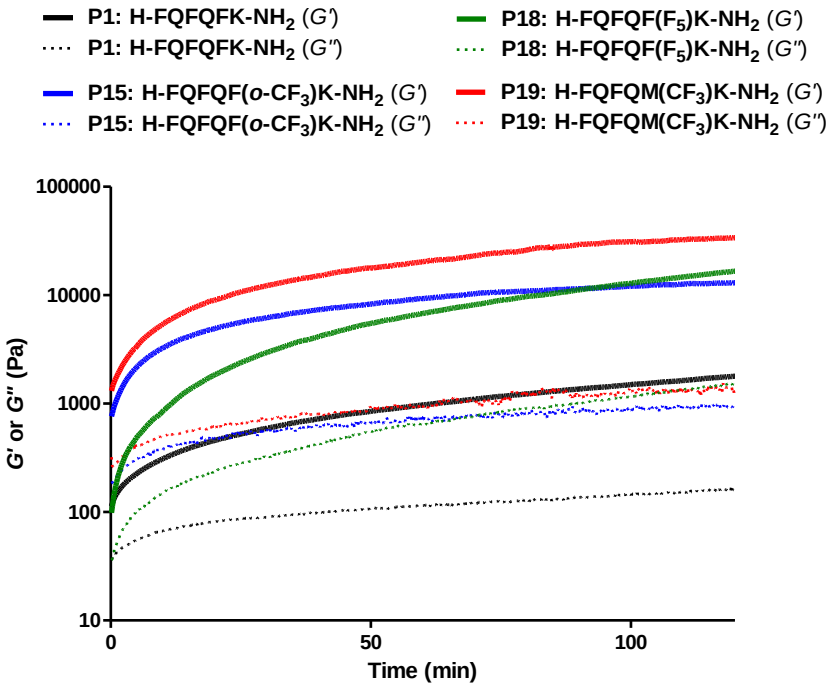

Figure 4. Rheological experiments (time sweep over 2 h) with average storage moduli (*G'*) and average loss moduli (*G''*) as a function of time, of hydrogels **P1**, **P15**, **P18** and **P19** at 2% w/v in PBS (n=3).

3.5. Characterization of the secondary structure

To verify that the designed amphipathic peptides self-assemble through β-sheets, Fourier-transform infrared spectroscopy (FT-IR) was performed. Data were collected within the amide I region (1600-1700 cm^{-1}), revealing hydrogen bonding between amide groups of the peptide backbones. An ion exchange procedure from the peptide TFA salt to the HCl salt was preliminary performed to avoid overlap of the TFA carbonyl signal (at 1672 cm^{-1}) with carbonyl signals of interest from the peptide (*See Supplementary Information Section S5.a*). As depicted in **Figures S18-S21**, most of the peptide hydrogels showed a characteristic intense signal of β-sheets around 1620 cm^{-1}.[77] To further confirm the β-sheet secondary structure occurring in the newly designed fluorinated hydrogels, circular dichroism was performed at 2% w/v in PBS (**Figure 5** & **S.I Figure S22-S25**). The spectrum observed for reference **P1** showed a maximum at 200 nm and a negative between 217 and 230 nm (**Figure 5**).

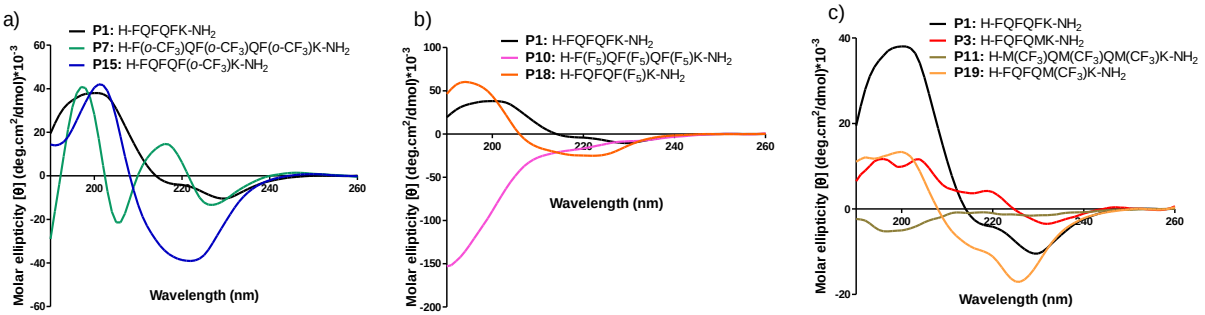

Figure 5. Circular dichroism spectra obtained at 2%w/v of: a) Phe(CF_3) peptides; b)Phe(F_5) peptides; c) Met(CF_3) peptides.

As can be seen in the electronic supporting information file (**Figure S22**), the spectra of the hydrogels containing monofluorinated phenylalanine (**P4-P6** and **P12-P14**) all indicated the presence of β-sheets. The intensities of the extrema tend to decrease along the fluorine position from *ortho>para>meta* in both sets of substitutions. This trend suggests that *meta* is the least

stabilizing position to induce clear β-sheet formation in the network. Notably, this observation correlates with the low *G'* value observed for the mechanical characterization of **P5**. However, for the hydrogels with Phe substituted in the *ortho* or *para* position, fluorine introduction seems to induce a positive impact on structuration with a more pronounced and defined β-sheet profile than the reference **P1**, even though their mechanical properties are similar.

In **Figure 5A**, **P15** displayed a typical β-sheet profile with a maximum at 201 nm and a minimum at 222 nm. However, its trisubstituted analogue **P7**, containing three *ortho*-trifluoromethyl phenylalanines, displayed a very different profile with several extrema that suggest an altered folding or a heterogenous conformer mixture. Similarly in **Figure 5B**, the profile of **P18**, containing one pentafluoro phenylalanine, showed more left-shifted extrema characteristics of parallel β-sheet signature, with a maximum at 194 nm and a minimum at 222 nm, while its trisubstituted analogue **P10** presented a more complex profile that does not fit with a classical β-sheet signature. These two cases suggest a correlation between the lack of β-sheet signature and the visual opacity of hydrogels **P7** and **P10**.

Hydrogels containing the Met(CF_3) amino acid (**Figure 5C**), **P19** presented a similar profile as the reference **P1,** although with lower intensity, while its trisubstituted analogue **P11** presented a random coil signature. This lack of structuration into β-sheets might be linked to the lack of aromaticity in this hydrogel, and its actual structuration might be different than for other aromatic analogues. A more clear cut image is obtained for **P19**, the monosubstituted analogue, that presented the best mechanical properties of the series and still gave a β-sheet signature, albeit less defined than for the reference **P1**, probably due to some structuration interferences through the trifluoromethionine lateral chains. However, its profile was still more defined than the one of **P3**,

the non-fluorinated analogue of **P19**, suggesting once more that the fluorinated group seems to help structuration.

3.6. Characterization of fiber morphology and self-assembled nanofibers network.

Based on previous characterization results, cryo- and negative stain TEM as well as atomic force microscopy (AFM) experiments were performed on hydrogel **P1** and on the selected fluorinated hydrogels **P15**, **P18** and **P19**, as they displayed the most interesting mechanical properties. The microscopy experiments were performed on hydrogels at 2% w/v or 0.1% w/v concentration, which allowed to visualize and characterize both the hydrogel network for assessment of fiber morphology, shedding light on the underpinning self-assembly (**Figure 6**). The images confirm that all samples were able to form an extensive network of nanofibers, with different densities, and fiber morphologies.

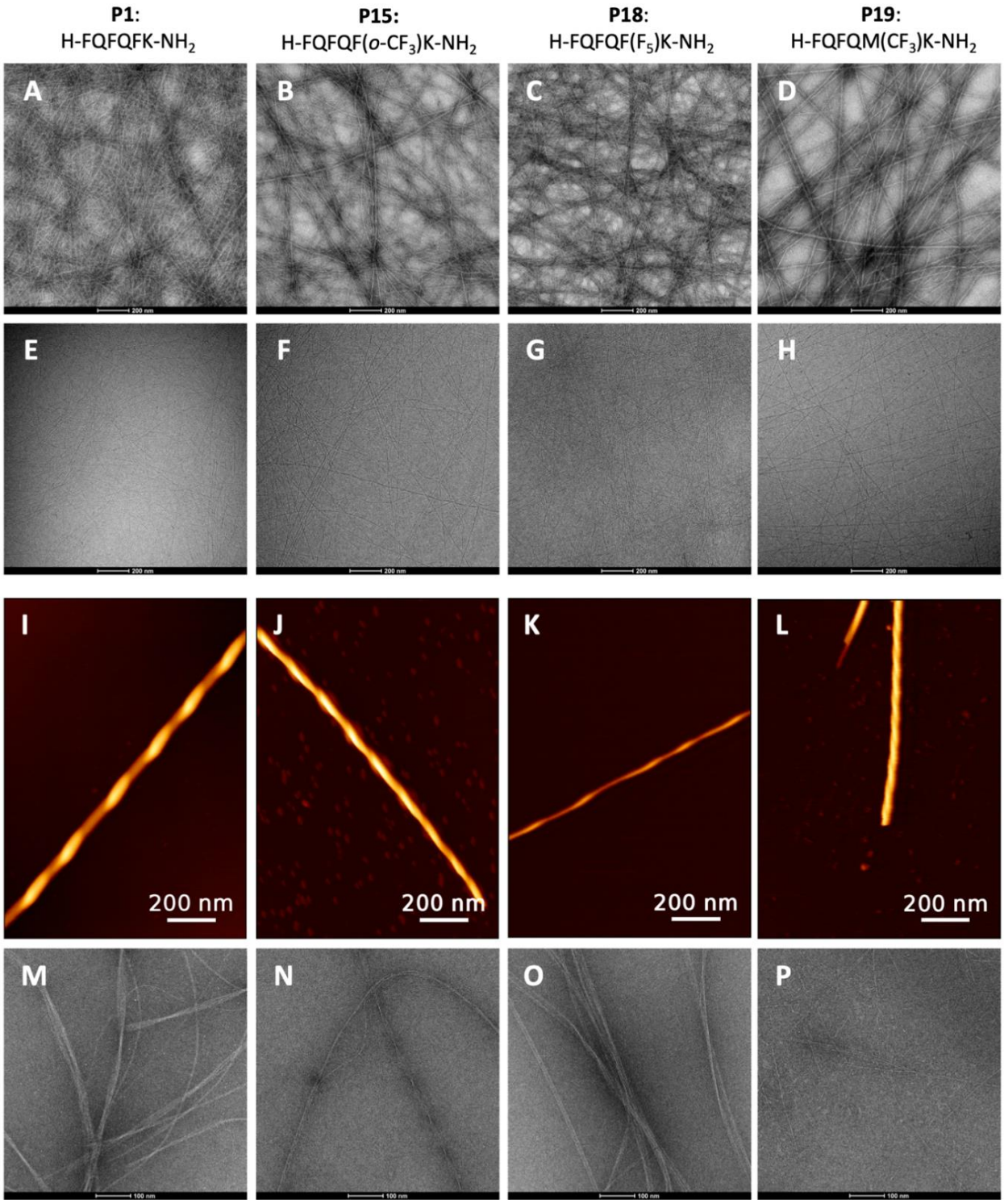

Q)	P1	P15	P18	P19
Fibril diameter (nm)	3.1 ± 1.1	4.7 ± 1.3	5.5 ± 1.6	4.3 ± 1.1

Fibre width (nm)	16.7 ± 4.6	15.5 ± 5.8	25.6 ± 8.9	11.0 ± 2.1
Fibre height (nm)	19.3 ± 4.5	14.5 ± 4.4	14.7 ± 5.6	11.6 ± 1.3
Pitch of twisted fibres (nm)	262.3 ± 50.4	138.0 ± 34.9	310.3 ± 96.2	n/a*

Figure 6. (A-D) Negatively stained TEM images of 2% w/v hydrogels; (E-H) cryo-TEM images of 2% w/v hydrogels; (I-L) AFM images of twisted fibres at 0.1% w/v; (M-P) Negatively stained TEM images of different fibre morphologies at 0.1% w/v. (Q) Dimensions of the fibrous morphologies at 0.1% w/v, presented as average ± SD (n ≥ 100). Widths are collected from the TEM images, heights from the AFM images and the pitch from both AFM and TEM data. The fibril diameter is an average of the width and height. *Due to the low presence of twisted fibres at 0.1% w/v and the polymorphism, a reliable pitch could not be measured.

As a reference, hydrogel **P1** showed similar morphologies as previously published, with the presence of mainly twisted fibres and bundled fibrils all over the network.[34,78] More precisely, fibrils with an average diameter of 3.1 ± 1.1 nm aligned with each other, forming a tape like structure of 16.7 ± 4.6 nm wide (**Figure 6M**). Additionally, the tape present left-handed twists (**Figure 6I**) of about 262.3 ± 50.4 nm, *i.e.* the pitch value. Those twisted fibres often further intertwine with each other (**Figure S26**).

Hydrogel **P15**, containing a Phe(*o*-CF_3), presented a dense network of tightly twisted fibres (width = 15.5 ± 5.8 nm, height = 14.5 ± 4.4 nm and pitch = 138.0 ± 34.9 nm). Remarkably, the twist is right-handed, as seen with the AFM experiments (**Figure 6J** and **Figure S27**), which is unusual for a peptide sequence with all amino acids in the *L*-configuration.[79] Thus, the *o*-CF_3 substituent strongly changes the self-assembly as compared to **P1**. The fibres are coexisting with small fibrils in the network of 4.7 ± 1.3 nm diameter (**Figure S28**).

Hydrogel **P18**, bearing a Phe(F_5), shows the formation of an entangled network at both 0.1% w/v and 2% w/v. Similar to **P1**, fibrils (with a diameter of 5.5 ± 1.6 nm) align with each other to form left-handed twisted fibres of variable dimensions, as seen on **Figure 6O**.

Hydrogel **P19**, containing Met(CF_3), presents the most polymorph fibres of the series; thick entangled fibres (**Figure 6L**) of 11.0 ± 2.1 nm in width are surrounded by loose fibrils (**Figure 6P**, **Figure S28**) with a diameter of 4.3 ± 1.1 nm. Some of the thicker fibres are tightly left-handed twisted with a minimal pitch of 49 nm. Locally, dense bundles of fibres are formed (**Figure S29**), which might contribute to the high *G'* obtained in the rheology experiments. Additionally, nucleation spheres were observed for both the 0.1% as 2% w/v sample (**Figure S30**), which may also promote the solid like behaviour for this hydrogel. The presence of unassembled peptide material caused the formation of a 2D-fibril network epitaxial to the mica lattice in the AFM experiments (**Figure S30c**).[80,81]

In general, these results confirm that the introduction of fluorine in the hexapeptide hydrogel does not prevent the formation of a dense nanofibrous network but imparts effects on the fibril alignments and twist characteristics. **P1** and **P18** have a similar appearance with the formation of aligned fibrils and large pitch values, while for **P15** and **P19** (with a CF_3 substitution present in both peptides), more bundled fibrils and more tightly twisted fibres, in combination with loose fibrils were observed.

3.7. *In vitro* release properties

Based on their mechanical properties and folding, peptide hydrogelators **P15**, **P18** and **P19** were chosen as the best candidates among the set of fluorinated peptides for further studies. In order to compare their controlled-release properties with the reference **P1**, *in vitro* release studies were performed with an opioid peptide cargo **C1**. Prior to this work, we studied the release of different

cargos from hydrogel **P1** and other analogues. Aiming at pain-killing management, we previously studied the release of conventional opioid drugs such as morphine and 14-MM, but also of opioid peptides like dermorphin or H-Dmt-D-Arg-Phe-Phe-NH_2 **C1**.[32,34,82] This latter cargo presented an interesting release profile from the cargo-loaded hydrogel **P1**.[33] Even though these *in vitro* experiments do not give a full representation of *in vivo* biological environments, it allows an estimation of the hydrogels' ability to retain a cargo. At the start of the experiment, PBS is added on top of a cargo-loaded hydrogel and the system is kept constant at a temperature of 37°C to simulate *in vivo* conditions.

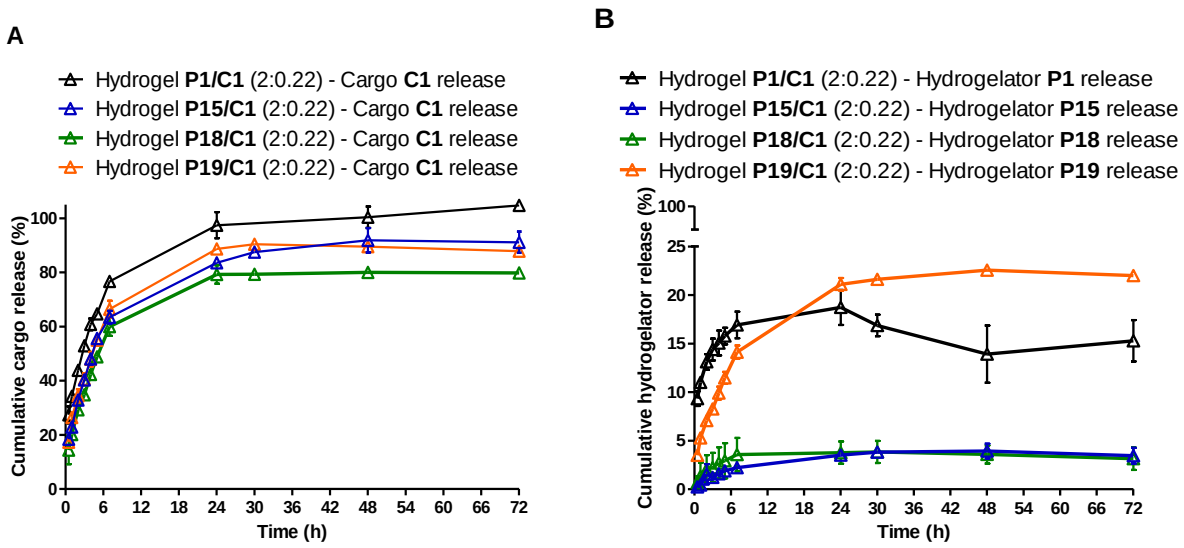

Figure 7. Curves of *in vitro* release of peptide cargo **C1** from 2% w/v peptide-hydrogels. The cargo is coformulated with the hydrogelator at a concentration of 0.22% w/v. Data points represent mean values with SD bars (n = 3). Measurement points are connected with lines to guide the eye. a) Release curves of cargo **C1** from **P1** (in black), **P15** (in blue), **P18** (in green) and **P19** (in orange) (2% w/v in PBS); b) Peptide-hydrogelator release from the hydrogel (same color attribution).

As can be seen in **Figure 7**, the four formulations present a very similar release profile of **C1** up to 24-48 h, with maximum released doses recorded up to 91%, 87% and 79% for **P15**, **P18** and

P19, respectively. However, it can be hypothesized that there is more cargo retention within fluorinated hydrogels as they present slightly lower plateau values compared to **P1**. However, when looking at **Figure 8b**, hydrogels **P15** and **P18** present a negligeable hydrogelator release from the gel (up to 3% after 72 h) in comparison to **P1** (up to 16% released) and **P19** (up to 22% released). We hypothesize that this *in vitro* gel stability can be related to the morphology of the underlying fibres and network, as **P15** and **P18** presented respectively tighter fibre twists and thicker fibre widths, as evidenced by TEM and AFM. This suggests that the fibre network in **P1** and **P19** is weaker than for **P15** and **P18**, that might present a slower gel erosion process according to **Figure 8b**, and potentially comprise superior cargo release systems.

3.8. *In vivo* gel stability by SPECT/CT imaging

After *in vitro* validation of fluorinated hydrogels **P15**, **P18** and **P19**, their *in vivo* gel stability was evaluated in mice using non-invasive SPECT/CT imaging. These were compared with previously published data on **P1**. For each hydrogelator, a DOTA chelator was coupled at the *N*-terminus of the hydrogelator sequence, with a βAla residue introduced as linker, resulting in peptides **P20**, **P21** and **P22** (respective analogues of **P15**, **P18** and **P19**).

The DOTA chelator was radiolabelled with the radioisotope ^{111}In. Each hydrogel was made up from 2% w/v hydrogelator in PBS, of which 0.1% w/v is DOTA-labelled, giving systems **P20**/**P15** (1:20); **P21**/**P18** (1:20) and **P22**/**P19** (1:20). After the subcutaneous injection of approximately 150 µL hydrogel just above the right hindlimb of mice and the integration of the radioactive signal allows to quantify the volume of gel remaining at the injection site (**Figure 8**). As a result, it appears that hydrogel **P20/P15** shows the highest *in vivo* gel stability, with 27% of the hydrogel still present at the injection site after one week, compared to 11% for the non-fluorinated reference **P1**. Hydrogels **P21/P18** and **P22/P19** present very similar profiles of stability as **P1**, but an

improved stability is apparent up to 1 day, with approximately 50% of fluorinated hydrogel volume still present after 6 h, higher than for **P1** that presented a volume of 38%. These results are in accordance with the *in vitro* gel stability observed for **P15** in **Figure 7**, while other systems **P21**/**P18** and **P22**/**P19** show more balanced correlation.

Additionally, monitoring the body-weight of the mice during the experiments indirectly indicates that these hydrogels represent safe systems for use in controlled-drug release applications, as all animals maintained normal physical appearance and behavior (**Figure S31**).

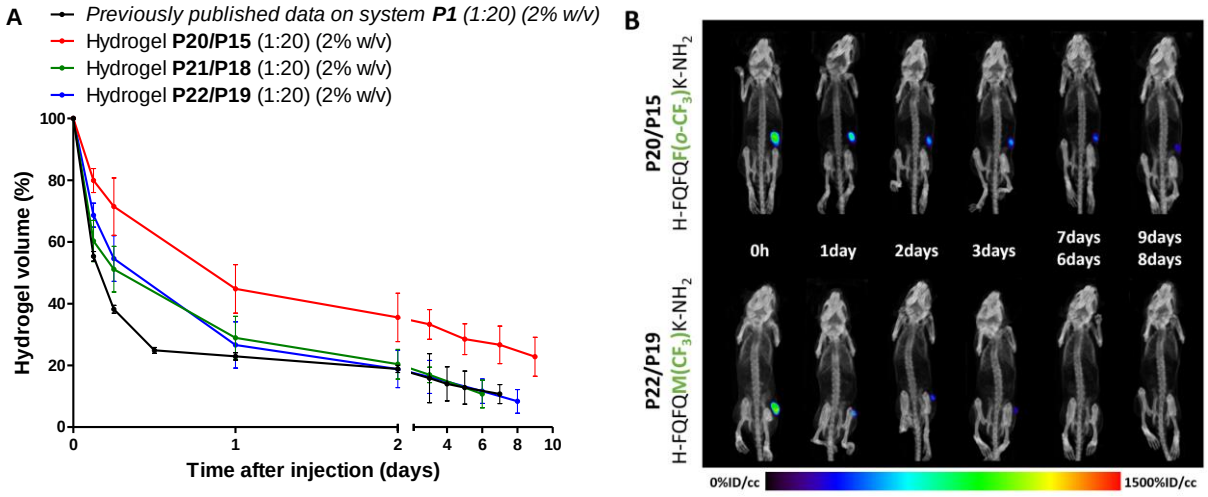

Figure 8. *In vivo* imaging of unloaded peptide-hydrogels, via nuclear SPECT/CT imaging after subcutaneous injection in mice. (**A**) *In vivo* stability profile of hydrogel **P20**/**P15** (1:20) (in red); **P21**/**P18** (1:20) (in green); **P22**/**P19** (1:20) (in blue) compared with previous data on **P1** (reference) (2% w/v in PBS of which 0.1% w/v is DOTA-labelled). The remaining radioactive signal at the injection site was quantified at different time-points post-injection, representing hydrogel stability over time. Data points presenting mean values ± SD (n = 3). (**B**) Representative SPECT/CT images taken at different time-points after subcutaneous injection of the hydrogels. All images were scaled to the same level (0–1500 %ID/cc).

CONCLUSIONS

In summary, we have investigated the introduction of fluorinated groups in our previous lead sequence **P1** and its effects on the hydrogel mechanical properties and secondary structure. As a result, we observed that the introduction of fluorine, along the hydrophobic face of the sequence, is limited to a certain range, as more rigid hydrogels were observed mostly when only one amino acid of the sequence is fluorinated. We also demonstrated that the introduction of a fluorinated group on a fully aliphatic 6-mer analogue sequence (**P2** and **P11**) counteracts the loss of π stacking interactions and leads to a system with mechanical properties close to **P1** properties. Rheological measurements on the set revealed the advantage of incorporating fluorine in the sequence to increase the gel stiffness, with storage moduli increases of up to ca. 18 times compared to the non-fluorinated reference. Further analysis of the influence of fluorine on fibre and network morphologies for three fluorinated system candidates (**P15**, **P18** and **P19**) showed promising physicochemical characteristics compared to the reference **P1**. Besides the thicker fibres observed for **P18**, it presents a similar network appearance as the reference, while **P15** and **P19**, bearing CF_3 groups, present more bundled fibrils with more tightly twisted fibres. Surprisingly, **P15** network presents very unusual right-handed twist, suggesting that the Phe(*o*-CF_3) substitution changes the assembly process completely. *In vitro* cargo release studies using an opioid peptide showed similar release profiles for each fluorinated hydrogel system, but **P15** and **P18** presented a lower hydrogelator release compared to the reference, suggesting a higher fibre stability that correlates with microscopy observations and thus suggest a potential slower gel erosion *in situ*. For hydrogel formulation **P20/P15**, this hypothesis was confirmed *in vivo* with gel stability experiments using SPECT/CT, which displayed a slower gel erosion in comparison with the previously published formulation of **P1**. In view of these promising results and a future potential use in the field of

therapeutics release, *in vivo* cargo release studies should be investigated on the fluorinated hydrogel **P15** (H-FQFQF(*o*-CF_3)K-NH_2) to verify its potential to slow-down the drug-release window obtained with the current reference system **P1**. Altogether, the current study proved that incorporation of fluorinated groups in the peptide hydrogelator allows to modulate the mechanical properties of the system and can help to slow down the gel erosion process *in vivo*.

ASSOCIATED CONTENT

Supporting Information.

The following files are available free of charge.

SI Honfroy et al Biomac 2024 (.doc)

AUTHOR INFORMATION

Corresponding Authors

*Steven Ballet: steven.ballet@vub.be

*Sophie Hernot: sophie.hernot@vub.be

*Grégory Chaume: gregory.chaume@cyu.fr

*Charlotte Martin: charlotte.martin@vub.be

Author Contributions

A.H. and A-M.T. conducted the peptide synthesis. A.H., J.Be., T.C., J.M., N.V.d.B., J.F.W. and J.G. conducted the hydrogel characterization experiments. A.H., performed the *in vitro* studies,

while A.H., and J.Br., carried out all the *in vivo* studies. S.B., C.M., G.C., T.B., N.L. and S.H. designed and coordinated the study. All authors contributed to the writing.

Funding Sources

We thank CY Initiative for their financial support through the EUTOPIA - PhD co-tutelle program 2020 (EXPLORE, 2020-166). We thank the CY Initiative of Excellence (grant « Investissements d'Avenir » ANR-16-IDEX-0008) for their financial support. SB and CM also acknowledge the Research Council of VUB for the financial support through the Strategic Research Programme (SRP50 and SRP95), and the financial support from the Wetenschappelijke Onderzoeksgemeenschap (WOG) "Supramolecular Chemistry and Materials" of the Research Foundation Flanders (FWO-V). JM thanks the Research Foundation – Flanders (FWO-Vlaanderen) for financial support (junior postdoctoral fellowship (1203524N)).

ACKNOWLEDGMENT

We thank CY Initiative for their financial support through the EUTOPIA - PhD co-tutelle program 2020 (EXPLORE, 2020-166). We thank the CY Initiative of Excellence (grant « Investissements d'Avenir » ANR-16-IDEX-0008) for their financial support. SB and CM also acknowledge the Research Council of VUB for the financial support through the Strategic Research Programme (SRP50 and SRP95), and the financial support from the Wetenschappelijke Onderzoeksgemeenschap (WOG) "Supramolecular Chemistry and Materials" of the Research Foundation Flanders (FWO-V). The authors thank TA Instruments for providing the Peltier Plate as well as Solvent Trap and Evaporation Blocker accessories. The authors thank Prof. Dr. Ronnie Willaert for the AFM assistance. AFM equipment has been funded by FWO grant number I002620. The authors would like to thank the lab technicians at ICMI Group (VUB) for taking care

of the animals during the *in vivo* experiments. The graphical abstract figure was created with Biorender.com. Dr. Guy Gouarin is acknowledged for his technical help on the electrostatic potential map modeling of Figure 2.

ABBREVIATIONS

PBS, phosphate-buffered solution; NMR, nuclear magnetic resonance; FT-IR, fourier-transform infrared spectroscopy; AFM, atomic force microscopy; CryoTEM, transmission electron cryomicroscopy; SPECT-CT, single-photon emission computed tomography x-ray computed tomography; SPPS, solid phase peptide synthesis; HBTU, *N*,*N*,*N*′,*N*′-Tetramethyl-*O*-(1H-benzotriazol-1-yl)uronium hexafluorophosphate; DIPEA, *N*,*N*-diisopropylethylamine; DMF, *N*,*N*-dimethylformamide; DOTA, dodecane tetraacetic acid; DCM, dichloromethane; TFA, trifluoroacetic acid; TIPS, triisopropylsilane; ACN, acetonitrile; DMSO, dimethylsulfoxide; RP-HPLC, reverse phase high performance liquid chromatography; HRMS, high-resolution mass spectrometry; MBq, megabecquerel; ITLC, instant thin layer chromatography; CD, circular dichroism; UV, ultraviolet; SD, standard deviation; PTA, phosphotungstic acid; AUC, area under the curve; %ID/cc, percentage of injected dose per cubic centimeter; ROI, region of interest; rt, retention time; 14-MM, 14-methoxymetopon; Dmt, 2′,6’-dimethyltyrosine.

REFERENCES

(1) Vargason, A. M.; Anselmo, A. C.; Mitragotri, S. The Evolution of Commercial Drug Delivery Technologies. *Nat. Biomed. Eng.* **2021**, *5* (9), 951–967.
(2) Adepu, S.; Ramakrishna, S. Controlled Drug Delivery Systems: Current Status and Future Directions. *Molecules* **2021**, *26* (19), 5905.
(3) Li, W.; Tang, J.; Lee, D.; Tice, T. R.; Schwendeman, S. P.; Prausnitz, M. R. Clinical Translation of Long-Acting Drug Delivery Formulations. *Nat. Rev. Mater.* **2022**, *7* (5), 406–420.
(4) Martin, C.; De Baerdemaeker, A.; Poelaert, J.; Madder, A.; Hoogenboom, R.; Ballet, S. Controlled-Release of Opioids for Improved Pain Management. *Mater. Today* **2016**, *19* (9), 491–502.

(5) Amabile, C. M.; Bowman, B. J. Overview of Oral Modified-Release Opioid Products for the Management of Chronic Pain. *Ann. Pharmacother.* **2006**, *40* (7–8), 1327–1335.
(6) Le, Z.; Yu, J.; Quek, Y. J.; Bai, B.; Li, X.; Shou, Y.; Myint, B.; Xu, C.; Tay, A. Design Principles of Microneedles for Drug Delivery and Sampling Applications. *Mater. Today* **2023**, *63*, 137–169.
(7) Prausnitz, M. R.; Langer, R. Transdermal Drug Delivery. *Nat. Biotechnol.* **2008**, *26* (11), 1261–1268.
(8) Storey, P.; Hill, H. H.; Louis, R. H. St.; Tarver, E. E. Subcutaneous Infusions for Control of Cancer Symptoms. *J. Pain Symptom Manage.* **1990**, *5* (1), 33–41.
(9) Stevens, R. A.; Ghazi, S. M. Routes of Opioid Analgesic Therapy in the Management of Cancer Pain. *Cancer Control* **2000**, *7* (2), 132–141.
(10) Liu, Q.; Das, M.; Liu, Y.; Huang, L. Targeted Drug Delivery to Melanoma. *Adv. Drug Deliv. Rev.* **2018**, *127*, 208–221.
(11) Kumari, P.; Ghosh, B.; Biswas, S. Nanocarriers for Cancer-Targeted Drug Delivery. *J. Drug Target.* **2016**, *24* (3), 179–191.
(12) Singh, R.; Lillard, J. W. Nanoparticle-Based Targeted Drug Delivery. *Exp. Mol. Pathol.* **2009**, *86* (3), 215–223.
(13) Liu, Y.-L.; Chen, D.; Shang, P.; Yin, D.-C. A Review of Magnet Systems for Targeted Drug Delivery. *J. Controlled Release* **2019**, *302*, 90–104.
(14) Seow, W. Y.; Hauser, C. A. E. Short to Ultrashort Peptide Hydrogels for Biomedical Uses. *Mater. Today* **2014**, *17* (8), 381–388.
(15) Yu, Z.; Cai, Z.; Chen, Q.; Liu, M.; Ye, L.; Ren, J.; Liao, W.; Liu, S. Engineering β-Sheet Peptide Assemblies for Biomedical Applications. *Biomater. Sci.* **2016**, *4* (3), 365–374.
(16) Jonker, A. M.; Löwik, D. W. P. M.; van Hest, J. C. M. Peptide- and Protein-Based Hydrogels. *Chem. Mater.* **2012**, *24* (5), 759–773.
(17) Park, K. Controlled Drug Delivery Systems: Past Forward and Future Back. *J. Controlled Release* **2014**, *190*, 3–8.
(18) Thambi, T.; Li, Y.; Lee, D. S. Injectable Hydrogels for Sustained Release of Therapeutic Agents. *J. Controlled Release* **2017**, *267*, 57–66.
(19) Fichman, G.; Gazit, E. Self-Assembly of Short Peptides to Form Hydrogels: Design of Building Blocks, Physical Properties and Technological Applications. *Acta Biomater.* **2014**, *10* (4), 1671–1682.
(20) Rizzo, F.; Kehr, N. S. Recent Advances in Injectable Hydrogels for Controlled and Local Drug Delivery. *Adv. Healthc. Mater.* **2021**, *10* (1), 2001341.
(21) Gulrez, S. K. H.; Al-Assaf, S.; Phillips, G. O. Hydrogels: Methods of Preparation, Characterization and Applications. In *Progress in Molecular and Environmental Bioengineering - From Analysis and Modeling to Technology Applications*; Carpi, A., Ed.; Intech, **2011**.
(22) Rivas, M.; Del Valle, L. J.; Alemán, C.; Puiggalí, J. Peptide Self-Assembly into Hydrogels for Biomedical Applications Related to Hydroxyapatite. *Gels* **2019**, *5* (1).
(23) La Manna, S.; Di Natale, C.; Onesto, V.; Marasco, D. Self-Assembling Peptides: From Design to Biomedical Applications. *Int. J. Mol. Sci.* **2021**, *22* (23), 12662.
(24) Oliveira, C. B. P.; Gomes, V.; Ferreira, P. M. T.; Martins, J. A.; Jervis, P. J. Peptide-Based Supramolecular Hydrogels as Drug Delivery Agents: Recent Advances. *Gels* **2022**, *8* (11), 706.

(25) Das, S.; Das, D. Rational Design of Peptide-Based Smart Hydrogels for Therapeutic Applications. *Front. Chem.* **2021**, *9*, 770102.
(26) Bowerman, C. J.; Nilsson, B. L. Review Self-Assembly of Amphipathic β-Sheet Peptides: Insights and Applications. *Pept. Sci.* **2012**, *98* (3), 169–184.
(27) Betush, R. J.; Urban, J. M.; Nilsson, B. L. Balancing Hydrophobicity and Sequence Pattern to Influence Self-Assembly of Amphipathic Peptides. *Pept. Sci.* **2018**, *110* (1), e23099.
(28) De Leon Rodriguez, L. M.; Hemar, Y.; Cornish, J.; Brimble, M. A. Structure–Mechanical Property Correlations of Hydrogel Forming β-Sheet Peptides. *Chem. Soc. Rev.* **2016**, *45* (17), 4797–4824.
(29) Zhang, S.; Holmes, T.; Lockshin, C.; Rich, A. Spontaneous Assembly of a Self-Complementary Oligopeptide to Form a Stable Macroscopic Membrane. *Proc. Natl. Acad. Sci. U. S. A.* **1993**, *90* (8), 3334–3338
(30) Mohammed, A.; Miller, A. F.; Saiani, A. 3D Networks from Self-Assembling Ionic-Complementary Octa-Peptides. *Macromol. Symp.* **2007**, *251* (1), 88–95.
(31) Bowerman, C. J.; Liyanage, W.; Federation, A. J.; Nilsson, B. L. Tuning β-Sheet Peptide Self-Assembly and Hydrogelation Behavior by Modification of Sequence Hydrophobicity and Aromaticity. *Biomacromolecules* **2011**, *12*(7), 2735–2745.
(32) Martin, C.; Oyen, E.; Wanseele, Y. V.; Haddou, T. B.; Schmidhammer, H.; Andrade, J.; Waddington, L.; Eeckhaut, A. V.; Mele, B. V.; Gardiner, J.; Hoogenboom, R.; Madder, A.; Spetea, M.; Ballet, S. Injectable Peptide-Based Hydrogel Formulations for the Extended in Vivo Release of Opioids. *Mater. Today Chem.* **2017**, *3*, 49–59.
(33) Martin, C.; Dumitrascuta, M.; Mannes, M.; Lantero, A.; Bucher, D.; Walker, K.; Van Wanseele, Y.; Oyen, E.; Hernot, S.; Van Eeckhaut, A.; Madder, A.; Hoogenboom, R.; Spetea, M.; Ballet, S. Biodegradable Amphipathic Peptide Hydrogels as Extended-Release System for Opioid Peptides. *J. Med. Chem.* **2018**, *61* (21), 9784–9789.
(34) Heremans, J., Chevillard, L., Mannes, M., Mangialetto, J., Leroy, K., White, J. F., Vinken, M., Gardiner, J., Van Mele, B., Van den Brande, N., Hoogenboom, R., Madder, A., Caveliers, V., Megarbane, B., Hernot, S., Ballet, S., & Martin, C. Impact of Doubling Peptide Length on in Vivo Hydrogel Stability and Sustained Drug Release. *J. Control. Release* **2022**, *350*, 514–524.
(35) Bettens, T.; Lacanau, V.; Lommel, R. V.; Maeseneer, T. D.; Vandeplassche, W.; Bertouille, J.; Brancart, J.; Barlow, T. M. A.; Woller, T.; Brande, N. V. den; Moldenaers, P.; Proft, F. D.; Madder, A.; Hoogenboom, R.; Martin, C.; Ballet, S.; Alonso, M. Towards the Understanding of Halogenation in Peptide Hydrogels: A Quantum Chemical Approach. *Mater. Adv.* **2021**, *2* (14), 4792–4803.
(36) Meanwell, N. A. Fluorine and Fluorinated Motifs in the Design and Application of Bioisosteres for Drug Design. *J. Med. Chem.* **2018**, *61* (14), 5822–5880.
(37) Grygorenko, O. O.; Melnykov, K. P.; Holovach, S.; Demchuk, O. Fluorinated Cycloalkyl Building Blocks for Drug Discovery. *ChemMedChem* **2022**, *17* (21), e202200365.
(38) Gillis, E. P.; Eastman, K. J.; Hill, M. D.; Donnelly, D. J.; Meanwell, N. A. Applications of Fluorine in Medicinal Chemistry. *J. Med. Chem*. **2015**, *58* (21), 8315–8359.
(39) Johnson, B. M.; Shu, Y.-Z.; Zhuo, X.; Meanwell, N. A. Metabolic and Pharmaceutical Aspects of Fluorinated Compounds. *J. Med. Chem.* **2020**, *63* (12), 6315–6386.
(40) Nair, A. S.; Singh, A. K.; Kumar, A.; Kumar, S.; Sukumaran, S.; Koyiparambath, V. P.; Pappachen, L. K.; Rangarajan, T. M.; Kim, H.; Mathew, B. FDA-Approved Trifluoromethyl Group-Containing Drugs: A Review of 20 Years. *Processes* **2022**, *10* (10), 2054.

(41) Gadais, C.; Devillers, E.; Gasparik, V.; Chelain, E.; Pytkowicz, J.; Brigaud, T. Probing the Outstanding Local Hydrophobicity Increases in Peptide Sequences Induced by Incorporation of Trifluoromethylated Amino Acids. *ChemBioChem* **2018**, *19* (10), 1026–1030.
(42) Hohmann, T.; Chowdhary, S.; Ataka, K.; Er, J.; Dreyhsig, G. H.; Heberle, J.; Koksch, B. Introducing Aliphatic Fluoropeptides: Perspectives on Folding Properties, Membrane Partition and Proteolytic Stability. *Chem. A Eur. J.* **2023**, *29* (23), e202203860.
(43) De Araujo, A. D.; Hoang, H. N.; Lim, J.; Mak, J. Y. W.; Fairlie, D. P. Tuning Electrostatic and Hydrophobic Surfaces of Aromatic Rings to Enhance Membrane Association and Cell Uptake of Peptides. *Angew. Chem.* **2022**, *134* (29), e202203995.
(44) Huhmann, S.; Koksch, B. Fine-Tuning the Proteolytic Stability of Peptides with Fluorinated Amino Acids: Fine-Tuning the Proteolytic Stability of Peptides with Fluorinated Amino Acids. *Eur. J. Org. Chem.* **2018**, *2018* (27–28), 3667–3679.
(45) Devillers, E.; Chelain, E.; Dalvit, C.; Brigaud, T.; Pytkowicz, (R)-α-Trifluoromethylalanine as a ^{19}F NMR Probe for the Monitoring of Protease Digestion of Peptides. *ChemBioChem* **2022**, *23* (1), e202100470.
(46) Marsh, E. N. G.; Suzuki, Y. Using ^{19} F NMR to Probe Biological Interactions of Proteins and Peptides. *ACS Chem. Biol.* **2014**, *9* (6), 1242–1250.
(47) Gimenez, D.; Phelan, A.; Murphy, C. D.; Cobb, S. L. ^{19}F NMR as a Tool in Chemical Biology. *Beilstein J. Org. Chem.* **2021**, *17*, 293–318.
(48) Gronenborn, A. M. Small, but Powerful and Attractive: ^{19}F in Biomolecular NMR. *Structure* **2022**, *30* (1), 6–14.
(49) Chowdhary, S.; Schmidt, R. F.; Sahoo, A. K.; Dieck, T. tom; Hohmann, T.; Schade, B.; Brademann-Jock, K.; Thünemann, A. F.; Netz, R. R.; Gradzielski, M.; Koksch, B. Rational Design of Amphiphilic Fluorinated Peptides: Evaluation of Self-Assembly Properties and Hydrogel Formation. *Nanoscale* **2022**, *14* (28), 10176–10189.
(50) Sloand, J. N.; Miller, M. A.; Medina, S. H. Fluorinated Peptide Biomaterials. *Pept. Sci.* **2021**, *113* (2), e24184.
(51) Tang, Y.; Ghirlanda, G.; Vaidehi, N.; Kua, J.; Mainz, D. T.; Goddard, W. A.; DeGrado, W. F.; Tirrell, D. A. Stabilization of Coiled-Coil Peptide Domains by Introduction of Trifluoroleucine. *Biochemistry* **2001**, *40* (9), 2790–2796.
(52) Tang, Y.; Tirrell, D. A. Biosynthesis of a Highly Stable Coiled-Coil Protein Containing Hexafluoroleucine in an Engineered Bacterial Host. *J. Am. Chem. Soc.* **2001**, *123* (44), 11089–11090.
(53) Wang, P.; Fichera, A.; Kumar, K.; Tirrell, D. A. Alternative Translations of a Single RNA Message: An Identity Switch of (2S,3R)-4,4,4-Trifluorovaline between Valine and Isoleucine Codons. *Angew. Chem. Int. Ed.* **2004**, *43* (28), 3664–3666.
(54) Bilgiçer, B.; Xing, X.; Kumar, K. Programmed Self-Sorting of Coiled Coils with Leucine and Hexafluoroleucine Cores. *J. Am. Chem. Soc.* **2001**, *123* (47), 11815–11816.
(55) Yoder, N. C.; Kumar, K. Fluorinated Amino Acids in Protein Design and Engineering. *Chem. Soc. Rev.* **2002**, *31* (6), 335–341.
(56) Marsh, E. N. G. Fluorinated Proteins: From Design and Synthesis to Structure and Stability. *Acc. Chem. Res.* **2014**, *47* (10), 2878–2886.
(57) Buer, B. C.; Meagher, J. L.; Stuckey, J. A.; Marsh, E. N. G. Structural Basis for the Enhanced Stability of Highly Fluorinated Proteins. *Proc. Natl. Acad. Sci.* **2012**, *109* (13), 4810–4815.

(58) Wang, Q.; Han, J.; Sorochinsky, A.; Landa, A.; Butler, G.; Soloshonok, V. A. The Latest FDA-Approved Pharmaceuticals Containing Fragments of Tailor-Made Amino Acids and Fluorine. *Pharmaceuticals* **2022**, *15* (8), 999.
(59) Mei, H.; Han, J.; Klika, K. D.; Izawa, K.; Sato, T.; Meanwell, N. A.; Soloshonok, V. A. Applications of Fluorine-Containing Amino Acids for Drug Design. *Eur. J. Med. Chem.* **2020**, *186*, 111826.
(60) Ryan, D. M.; Anderson, S. B.; Senguen, F. T.; Youngman, R. E.; Nilsson, B. L. Self-Assembly and Hydrogelation Promoted by F_5 -Phenylalanine. *Soft Matter* **2010**, *6* (3), 475–479.
(61) Ryan, D. M.; Anderson, S. B.; Nilsson, B. L. The Influence of Side-Chain Halogenation on the Self-Assembly and Hydrogelation of Fmoc-Phenylalanine Derivatives. *Soft Matter* **2010**, *6* (14), 3220.
(62) Aviv, M.; Cohen-Gerassi, D.; Orr, A. A.; Misra, R.; Arnon, Z. A.; Shimon, L. J. W.; Shacham-Diamand, Y.; Tamamis, P.; Adler-Abramovich, L. Modification of a Single Atom Affects the Physical Properties of Double Fluorinated Fmoc-Phe Derivatives. *Int. J. Mol. Sci.* **2021**, *22* (17), 9634.
(63) Tiwari, P.; Gupta, A.; Mehra, R. R.; Khan, N.; Harjit, J.; Ashby, C. R.; Basu, A.; Tiwari, A. K.; Singh, M.; Dutt Konar, A. Fluorinated Diphenylalanine Analogue Based Supergelators: A Stencil That Accentuates the Sustained Release of Antineoplastic Drugs. *Supramol. Chem.* **2020**, *32* (9), 495–507.
(64) Wang, Y.; Zhang, Z.; Xu, L.; Li, X.; Chen, H. Hydrogels of Halogenated Fmoc-Short Peptides for Potential Application in Tissue Engineering. *Colloids Surf. B Biointerfaces* **2013**, *104*, 163–168.
(65) Truong, W. T.; Su, Y.; Gloria, D.; Braet, F.; Thordarson, P. Dissolution and Degradation of Fmoc-Diphenylalanine Self-Assembled Gels Results in Necrosis at High Concentrations in Vitro. *Biomater. Sci.* **2015**, *3* (2), 298–307.
(66) Abraham, B. L.; Liyanage, W.; Nilsson, B. L. Strategy to Identify Improved N-Terminal Modifications for Supramolecular Phenylalanine-Derived Hydrogelators. *Langmuir* **2019**, *35* (46), 14939–14948.
(67) Hsu, S.-M.; Lin, Y.-C.; Chang, J.-W.; Liu, Y.-H.; Lin, H.-C. Intramolecular Interactions of a Phenyl/Perfluorophenyl Pair in the Formation of Supramolecular Nanofibers and Hydrogels. *Angew. Chem. Int. Ed.* **2014**, *53* (7), 1921–1927.
(68) Wu, F.-Y.; Hsu, S.-M.; Cheng, H.; Hsu, L.-H.; Lin, H.-C. The Effect of Fluorine on Supramolecular Hydrogelation of 4-Fluorobenzyl-Capped Diphenylalanine. *New J. Chem.* **2015**, *39* (6), 4240–4243.
(69) Saddik, A. A.; Chakravarthy, R. D.; Mohammed, M.; Lin, H.-C. Effects of Fluoro Substitutions and Electrostatic Interactions on the Self-Assembled Structures and Hydrogelation of Tripeptides: Tuning the Mechanical Properties of Co-Assembled Hydrogels. *Soft Matter* **2020**, *16* (44), 10143–10150.
(70) Ravarino, P.; Di Domenico, N.; Barbalinardo, M.; Faccio, D.; Falini, G.; Giuri, D.; Tomasini, C. Fluorine Effect in the Gelation Ability of Low Molecular Weight Gelators. *Gels* **2022**, *8* (2), 98.
(71) Bowerman, C. J.; Ryan, D. M.; Nissan, D. A.; Nilsson, B. L. The Effect of Increasing Hydrophobicity on the Self-Assembly of Amphipathic β-Sheet Peptides. *Mol Biosyst* **2009**, *5* (9), 1058–1069.

(72) Monkovic, J. M.; Gibson, H.; Sun, J. W.; Montclare, J. K. Fluorinated Protein and Peptide Materials for Biomedical Applications. *Pharmaceuticals* **2022**, *15* (10), 1201.
(73) Wheeler, S. E.; Houk, K. N. Through-Space Effects of Substituents Dominate Molecular Electrostatic Potentials of Substituted Arenes. *J. Chem. Theory Comput.* **2009**, *5* (9), 2301–2312.
(74) Hansch, C.; Leo, A.; Unger, S. H.; Kim, K. H.; Nikaitani, D.; Lien, E. J. Aromatic Substituent Constants for Structure-Activity Correlations. *J. Med. Chem.* **1973**, *16* (11), 1207–1216.
(75) Hansch, Corwin.; Leo, A.; Taft, R. W. A Survey of Hammett Substituent Constants and Resonance and Field Parameters. *Chem. Rev.* **1991**, *91* (2), 165–195.
(76) Yan, C.; Pochan, D. J. Rheological Properties of Peptide-Based Hydrogels for Biomedical and Other Applications. *Chem. Soc. Rev.* **2010**, *39* (9), 3528.
(77) Zandomeneghi, G.; Krebs, M. R. H.; McCammon, M. G.; Fändrich, M. FTIR Reveals Structural Differences between Native β-sheet Proteins and Amyloid Fibrils. *Protein Sci.* **2004**, *13* (12), 3314–3321.
(78) De Maeseneer, T.; Cauwenbergh, T.; Gardiner, J.; White, J. F.; Thielemans, W.; Martin, C.; Moldenaers, P.; Ballet, S.; Cardinaels, R. Peptide Sequence Variations Govern Hydrogel Stiffness: Insights from a Multi-Scale Structural Analysis of H-FQFQFK-NH_2 Peptide Derivatives. *Macromol. Biosci.* **2024**, 2300579.
(79) Zheng, Y.; Mao, K.; Chen, S.; Zhu, H. Chirality Effects in Peptide Assembly Structures. *Front. Bioeng. Biotechnol.* **2021**, *9*, 703004.
(80) Li, H.; Zhang, F.; Zhang, Y.; Ye, M.; Zhou, B.; Tang, Y.-Z.; Yang, H.-J.; Xie, M.-Y.; Chen, S.-F.; He, J.-H.; Fang, H.-P.; Hu, J. Peptide Diffusion and Self-Assembly in Ambient Water Nanofilm on Mica Surface. *J. Phys. Chem. B* **2009**, *113* (26), 8795–8799.
(81) Bertouille, J.; Kasas, S.; Martin, C.; Hennecke, U.; Ballet, S.; Willaert, R. G. Fast Self-Assembly Dynamics of a β-Sheet Peptide Soft Material. *Small* **2023**, *19* (20), 2206795.
(82) Oyen, E.; Martin, C.; Caveliers, V.; Madder, A.; Van Mele, B.; Hoogenboom, R.; Hernot, S.; Ballet, S. *In Vivo* Imaging of the Stability and Sustained Cargo Release of an Injectable Amphipathic Peptide-Based Hydrogel. *Biomacromolecules* **2017**, *18* (3), 994–1001.